

ISTANBUL TECHNICAL UNIVERSITY ★ GRADUATE SCHOOL OF SCIENCE
ENGINEERING AND TECHNOLOGY

**NUMERICAL INVESTIGATION OF CRAH BYPASS IN THE
AIR-COOLED DATA CENTERS**



M.Sc. THESIS

Vahid Ebrahimpour Ahmadi

Department of Mechanical Engineering

Heat and Fluid Programme

MAY 2019

**NUMERICAL INVESTIGATION OF CRAH BYPASS IN THE
AIR-COOLED DATA CENTERS**

M.Sc. THESIS

**Vahid Ebrahimpour Ahmadi
(503161154)**

Department of Mechanical Engineering

Heat and Fluid Programme

Thesis Advisor: Dr. Sertaç Çadırcı

Co-advisor: Dr. Hamza Salih Erden

MAY 2019

**HAVA İLE SOĞUTULMUŞ VERİ MERKEZLERİNDE KLİMA BAYPAS
YÖNTEMİNİN SAYISAL ARAŞTIRMASI**

YÜKSEK LİSANS TEZİ

**Vahid Ebrahimpour Ahmadi
(503161154)**

Makine Mühendisliği Anabilim Dalı

Isı-Akışkan Programı

**Tez Danışmanı: Dr. Sertaç Çadircı
Eş Danışman: Dr. Hamza Salih Erden**

MAYIS 2019

Vahid Ebrahimpour Ahmadi, a M.Sc. student of ITU Graduate School of Science Engineering and Technology 503161154 successfully defended the thesis entitled “NUMERICAL INVESTIGATION OF CRAH BYPASS IN THE AIR-COOLED DATA CENTERS”, which he/she prepared after fulfilling the requirements specified in the associated legislations, before the jury whose signatures are below.

Thesis Advisor : **Dr. Sertaç Çadırcı**
Istanbul Technical University

Co-advisor : **Dr. Hamza Salih Erden**
Istanbul Technical University

Jury Members : **Dr. Ersin Sayar**
Istanbul Technical University

Prof. Dr. Mehmet Arık
Özyeğin University

Prof. Dr. Hakan Demir
Yıldız Technical University

Date of Submission : **3 May 2019**

Date of Defense : **29 May 2019**



FOREWORD

I would like to express my gratitude to my co-advisor Dr. Hamza Salih Erden who persistently helped me and without his guidance this thesis would not have been prepared. I really thank my advisor Dr. Sertac Cadirci for his suggestions and encouragement during this study. I would like to thank İsmail Türkmen, as a good friend was always willing to help during my thesis. I appreciate the The Scientific and Technological Research Council of Turkey (TUBITAK) for supporting this study under the 118M238 project ID number. Moreover, the experimental data used in this paper were measured by M.Koz and M.T. Yildirim at the Syracuse University Green Data Center Research Laboratory under NYSERDA award 41202. The authors are indebted to Prof. H. E. Khalifa, who was the Principal Investigator of this award, for allowing us access to these measurements.

Last but not the least, I would like to express the deepest appreciation to my parents and family for supporting me spiritually throughout my studies and life.

May 2019

Vahid Ebrahimpour Ahmadi
(Master of science student)



TABLE OF CONTENTS

| | <u>Page</u> |
|---|-------------|
| FOREWORD | vii |
| TABLE OF CONTENTS | ix |
| ABBREVIATIONS | xi |
| SYMBOLS | xiii |
| LIST OF TABLES | xv |
| LIST OF FIGURES | xvii |
| SUMMARY | xix |
| ÖZET | xxi |
| 1. INTRODUCTION | 1 |
| 1.1 Background..... | 1 |
| 1.2 Literature Review | 3 |
| 1.3 Hypothesis | 7 |
| 1.4 Objectives | 8 |
| 2. THEORY | 11 |
| 2.1 Governing Equations | 11 |
| 2.2 Turbulence Modeling..... | 13 |
| 2.3 Near Wall Treatment..... | 14 |
| 2.4 Buoyancy | 15 |
| 3. METHODOLOGY | 17 |
| 3.1 CFD | 17 |
| 3.1.1 Grid independency..... | 20 |
| 3.2 TDM | 21 |
| 3.3 Optimization..... | 23 |
| 3.4 Model Assumptions..... | 24 |
| 4. MODEL VALIDATION | 27 |
| 5. RESULTS AND DISCUSSION | 35 |
| 5.1 CFD Versus TDM For The Optimization Of The Baseline QDC | 35 |
| 5.2 Parametric Analysis..... | 37 |
| 5.2.1 Plenum height..... | 37 |
| 5.2.2 IT load and servers airflow temperature increase variations | 38 |
| 6. CONCLUSIONS | 45 |
| REFERENCES | 47 |
| CURRICULUM VITAE | 51 |



ABBREVIATIONS

| | |
|--------------|--------------------------------------|
| BL | : baseline |
| BP | : bypass |
| CA | : cold aisle |
| CFD | : computational fluid dynamics |
| COP | : coefficient of performance |
| CRAH | : computer room air handling/handler |
| EA | : enclosed aisle |
| fBP | : forced CRAH bypass |
| FNM | : flow network model |
| GDCRL | : green data center research lab |
| HA | : hot aisle |
| HX | : heat exchanger |
| iBP | : induced CRAH bypass |
| IT | : information technology |
| NTU | : number of transfer units |
| PUE | : Power usage effectiveness |
| QDC | : quadrant data center |
| TDM | : thermodynamics modeling |
| BP | : bypass |
| CA | : cold aisle |
| BL | : baseline |
| BP | : bypass |
| CA | : cold aisle |



SYMBOLS

| | |
|------------|-----------------------------------|
| b | : bias |
| bp | : bypass |
| ch | : chiller |
| chw | : chilled water |
| cr | : CRAH |
| fan | : fan |
| i | : inlet |
| K | : loss coefficient |
| max | : maximum |
| o | : outlet |
| p | : precision |
| p | : pressure, Pa |
| r | : rack |
| T | : temperature, °C |
| u | : uncertainty |
| UA | : thermal conductance, kW/K |
| V | : velocity, m/s |
| W | : power, kW |
| Δ | : difference |
| ε | : thermal effectiveness |
| ρ | : mass density, kg/m ³ |
| φ | : velocity, m/s |



LIST OF TABLES

| | <u>Page</u> |
|---|-------------|
| Table 3.1 : Summary of Model Assumptions..... | 25 |
| Table 4.1 : Calculation of bias error over the server inlets..... | 30 |
| Table 4.2 : Total uncertainty error calculation over the server inlets. | 30 |
| Table 4.3 : Total uncertainty error calculation for leakage tiles. | 31 |





LIST OF FIGURES

| | <u>Page</u> |
|---|-------------|
| Figure 1.1 : Schematic of chilled water cycle and airflow loop in a raised-floor data center [3]. | 2 |
| Figure 1.2 : Recommended range for data processing environments by ASHRAE. | 2 |
| Figure 1.3 : Generic OA and EA data centers (www.42u.com)..... | 3 |
| Figure 1.4 : Representative view of (a) induced and (b) forced BP configurations for air-cooled data centers. | 7 |
| Figure 3.1 : Top view of the QDC layout for both (a) iBP and (b) fBP configurations..... | 18 |
| Figure 3.2 : Heating up cold airflow through the server racks. | 19 |
| Figure 3.3 : Separating walls above the BP fan surfaces. | 19 |
| Figure 3.4 : Airflow pattern with applying swirl-velocity specification. | 20 |
| Figure 3.5 : Temperature variation of a particular point at the entrance of the CRAH unit in different number of cells. | 21 |
| Figure 3.6 : Temperature contours of rack inlets in different number of cells..... | 22 |
| Figure 3.7 : Schematics of TDM and FNM. | 22 |
| Figure 3.8 : Outline of TDM-based and CFD-based optimization. | 23 |
| Figure 4.1 : Experimental facility (a) layout, and (b) CFD model..... | 28 |
| Figure 4.2 : Pictures of GDCRL (a) thermocouple frames, (b) portable cold aisle containment, and (c) installed fans below the perforated tiles in CA | 29 |
| Figure 4.3 : Airflow exit area for three different cases (a) case 1, (b) case 2, and (c) case 3. | 31 |
| Figure 4.4 : Comparison of experimental and CFD temperatures for (a) case 1, (b) case 2, and (c) case 3..... | 32 |
| Figure 5.1 : Temperature contours of (a) case 2, and (b) case 1. | 35 |
| Figure 5.2 : Comparison of cooling power between CFD cases and TDM in iBP configuration. | 36 |
| Figure 5.3 : Comparison of cooling power between CFD cases and TDM in fBP configuration. | 36 |
| Figure 5.4 : Pressure distribution at the plenum floor for (a) 36-inch, (b) 28-inch, and (c) 20-inch plenum heights. | 38 |
| Figure 5.5 : Variation of plenum height for iBP configuration (a) EA and (b) OA data centers. | 39 |
| Figure 5.6 : Variation of plenum height for fBP configuration (a) EA and (b) OA data centers. | 40 |
| Figure 5.7 : Comparison of cooling power for $\Delta T = 20^{\circ}\text{C}$ by TDM and CFD in iBP configuration. | 41 |

Figure 5.8 : Comparison of cooling power in iBP configuration for various (a) IT loads and (b) servers airflow rates. 42

Figure 5.9 : Comparison of cooling power in fBP configuration for various (a) IT loads and (b) servers airflow rates. 43



NUMERICAL INVESTIGATION OF CRAH BYPASS IN THE AIR-COOLED DATA CENTERS

SUMMARY

Aisle containment decreases the temperature non-uniformities across the server rack inlets in air-cooled data centers and allows higher temperature operation. Higher operating temperature not only enhances the cooling system efficiency but also increases the possibility of free cooling. Enclosed aisle does not ensure the lowest cooling power in data centers. Actually, computer room air handler (CRAH) fans need to supply the entire required rack airflow as well as leakage flow, which naturally exists between plenum and room, and hence CRAH fans form noticeable part of cooling power. CRAH bypass (BP) method employs additional fans installed under the perforated tiles to provide a fraction of server racks' required airflow either by inducing or forcing room air through the low flow resistance BP tiles or leakage paths. This method reduces the airflow across high flow resistance components of CRAH units. Although the CRAH BP method decreases the total fan power in the data center, the chiller power increases due to lower temperature operation since the room supplies some fraction of hot air to the plenum. The reduced-order modeling tools in the literature adequately predicting the fan power assume well-mixed temperature at rack inlets to deal with this optimization problem and fail to quantify the impact of ignoring temperature non-uniformities. This study includes an experimental verification of CFD modeling for CRAH BP method in predicting temperatures in a data center test cell. This part investigates impact of various modeling parameters in order to find the most appropriate CFD simulation and determines the geometry details as the most powerful factor in improving CFD results. The performed CFD verification provides guidelines for the modeling and optimization effort using CFD. Available CFD simulations have been carried out by using commercial CFD software Ansys Fluent 18.1. The subsequent parametric study uses both CFD and reduced-order modeling tools on a more representative quadrant of a large data center to investigate induced and forced CRAH BP in both enclosed and open aisle configurations as well as comparing various plenum heights, IT load and server airflow rate. Results indicate where reduced-order modeling tools perform reasonably well and where the need for CFD starts to emerge, and identify various favorable data center designs and operating conditions for CRAH BP method.



HAVA İLE SOĞUTULMUŞ VERİ MERKEZLERİNDE KLİMA BAYPAS YÖNTEMİNİN SAYISAL ARAŞTIRMASI

ÖZET

Bir veri merkezi, verilerin işlenmesi ve saklanması amacıyla sunucu raflarından oluşan bir tesistir. Tüm dünyada, özellikle ABD'deki veri merkezleri, enerji tüketiminin önemli bir bölümünü oluşturur. Yakın bir araştırmaya [1] dayanarak, 2014 yılında, ABD'deki veri merkezlerinin hesapladığı güç kullanımı yaklaşık 70 milyar kWh veya toplam ABD elektrik tüketiminin yaklaşık %1.8 'i kadardı. Bu çalışma 2010-2014 yılları arasında veri merkezleri tarafından tüketilen elektriğin yaklaşık %4, ve 2005'ten 2010'a kadar % 24 arttığını göstermektedir. Veri merkezlerinde 2014'ten 2020'ye kadar elektrik tüketiminin bu yükselen trendi sürdürmesi beklenmektedir. Bu nedenle, veri merkezlerinin enerji verimliliğini arttırmak için çok çabaya ihtiyaç duyulur.

Veri merkezlerinde soğutma sistemleri tarafından yapılan enerji tüketimi, toplam enerji kullanımının yarısını oluşturabilir ve toplam işletme maliyetlerine önemli ölçüde katkıda bulunur. Bu nedenle, soğutma sistemlerinin güç kullanımını azaltmak, veri merkezlerinin enerji verimliliğini iyileştirmede önemli bir parametre olarak kabul edilebilir. Tipik bir veri merkezinde, soğutma talebini karşılamak için genellikle soğutulmuş bir su sistemi ve bir hava akımı döngüsü kullanılır. Sonuç olarak, etkili hava akışı yönetimi ile birlikte optimize edilmiş bir soğutulmuş su sistemi, sadece enerji tüketimini ve emisyonu azaltmakla kalmaz, aynı zamanda IT ekipmanının güvenilir çalışmasını sağlar [2].

Genellikle hava soğutmalı veri merkezleri sert veya yükseltilmiş zemin düzeninde oluşur ve sunucu rafları tipik olarak sıcak ve soğuk koridorlar oluşturmak için hava soğutmalı veri merkezlerinde arka arkaya ve önden öne yerleştirilir. Şekil 1.3, genel bir açık soğuk koridor (OA) ve kapalı koridor (EA) veri merkezinin şemalarını göstermektedir. Yükseltilmiş zemin yapılandırmasında veri merkezindeki CRAH / CRAC (bilgisayar odası klima santrali) üniteleri, yer altı plenumundan soğuk koridorlara soğuk hava akışı sağlar ve ısıtılmış havayı sıcak koridorlardan çeker. Hava akış alanı veri merkezinin soğutulmasını etkilediğinden, yüksek güç yoğunluğu ve termal yüklerde sıcaklık ve akış alanlarının izlenmesi kritik. Hesaplamalı akışkanlar dinamiği (CFD), düşük maliyetli hava akış yollarının yanı sıra çeşitli noktaların sıcaklığı hakkında ayrıntılı bilgi göstermek için güçlü bir araçtır.

Kapalı koridor, hava soğutmalı veri merkezlerinde sunucu kabinlerinin girişlerindeki sıcaklık homojenliğini azaltır ve daha yüksek sıcaklıkta çalışma sağlar. Daha yüksek çalışma sıcaklığı sadece soğutma sistemi verimliliğini arttırmaz, aynı zamanda serbest soğutma olasılığını da artırır. Kapalı koridor, veri merkezlerinde en düşük soğutma gücünü sağlamaz. Aslında, bilgisayar odası hava taşıyıcı (CRAH) fanlarının, gerekli tüm raf hava akışının yanı sıra, plenum ve oda arasında doğal olarak bulunan sızıntı akışını da sağlamaları gerekir ve bu nedenle CRAH fanları, soğutma gücünün belirgin bir bölümünü oluşturur. CRAH bypass (BP) yöntemi, düşük akış dirençli BP karoları

veya sızıntı yollarına oda havasını indükleyerek veya zorlayarak sunucu raflarının gerekli hava akışının bir kısmını sağlamak için delikli fayansların altına monte edilmiş ek fanları kullanır. Bu yöntem, CRAH ünitelerinin yüksek akış direnci bileşenlerinde hava akışını azaltır. Her ne kadar CRAH BP yöntemi, veri merkezindeki toplam fan gücünü düşürse de, oda plenuma bir miktar sıcak hava sağladığından, düşük sıcaklık çalışması nedeniyle soğutucu gücü artar. Literatürdeki azaltılmış dereceli modelleme araçları, fan gücünü yeterli bir şekilde öngörerek, bu optimizasyon problemi ile başa çıkmak için raf girişlerinde iyi bir şekilde karıştırılmış bir sıcaklığa sahip olduğunu kabul etmekte ve görmezlikteki sıcaklığın homojen olmamalarının etkisini ölçmekte başarısız olmaktadır.

Bu çalışma, bir veri merkezi test hücreesindeki sıcaklıkları öngörmede CRAH BP yöntemi için CFD modellemesinin deneysel bir doğrulamasını içerir. Bu bölüm, en uygun CFD simülasyonunu bulmak için çeşitli modelleme parametrelerinin etkisini araştırmakta ve CFD sonuçlarını iyileştirmede geometri detaylarını en güçlü faktör olarak belirlemektedir. Yapılan CFD doğrulama, CFD kullanarak modelleme ve optimizasyon çabası için kılavuzlar sağlar. Kullanılabilir CFD simülasyonları, ticari CFD yazılımı Ansys Fluent 18.1 kullanılarak yapıldı. Takip eden parametrik çalışma, hem kapalı hem de açık koridor konfigürasyonlarında indüklenen ve zorlanan CRAH BP'yi araştırmanın yanı sıra çeşitli plenum yüksekliklerini, IT yükünü ve sunucu hava akışını karşılaştırmanın yanı sıra, hem kapalı hem de açık koridor konfigürasyonlarında araştırmak için hem CFD hem de indirgenmiş modelleme (TDM) araçlarını kullanır. Sonuçlar, düşük sipariş modelleme araçlarının nerede oldukça iyi performans gösterdiğini ve CFD ihtiyacının ortaya çıkmaya başladığı yerleri göstermektedir ve CRAH BP yöntemi için çeşitli uygun veri merkezi tasarımlarını ve çalışma koşullarını tanımlamaktadır.

Şekil 3.7 iki adımlı akış ve enerji modelleme yaklaşımını özetlemektedir. Bu kapsamda akış ağı modellemesi (FNM) için ticari bir ürün olan AFT Fathom adlı yazılım kullanılacaktır. Bu yazılım ile oluşturulan akış ağı modelleri CRAH BP yöntemi uygulaması yapılan deneysel bir veri merkezinde deneysel olarak teyit edilmiştir [25][26]. Hızlı çalışması nedeniyle FNM, optimizasyon çalışmasına çok daha yatkın bir araç olduğu için bu çalışma kapsamında da optimizasyon çalışmalarının temelini oluşturacaktır. Zira FNM CRAH ve BP fan gücü değerlerini detaylı CFD çalışmalarına gerek duymadan tahmin eder. FNM fan gücü tahminlerinde oldukça başarılı sonuçlar verirken, bu sonuçları değerlendiren indirgenmiş model yaklaşımının (TDM) özellikle yüksek BP akışlarında sıcaklık dağılımındaki düzensizliklerin artmasıyla hangi şartlarda güvenilir sonuçlar vermekten uzaklaştığı ancak detaylı CFD modelleriyle görülebilecektir. Eksiksiz bir analiz için fanlar dışında soğutma altyapısının güç gereksiniminin de gerçekçi bir yaklaşımla tahmin edilebilmesi gerekir. Bu çalışmada TRNSYS adlı yazılım kullanılarak veri merkezi soğutma altyapısının temel bileşenlerine ait güç kullanımları (chiller, soğutma kulesi, pompalar, fanlar vb.) ve oda seviyesinde önemli noktadaki sıcaklıklar mükemmel karışım varsayımıyla tespit edilecektir. CRAH BP çalışması esnasında artış gösteren ve CFD ile tespit edilecek sıcaklık düzensizlikleri mükemmel karışım varsayımının güvenilirliğini test edecek, gereken yerlerde düzeltmelerin yapılabilmesini sağlayacaktır.

Bu araştırma kapalı koridorlu (EA) veri merkezlerinde enerji verimliliğini arttırmak amacıyla önerilen CRAH baypas (BP) yönteminin hem EA hem de açık koridorlu (OA) veri merkezlerindeki akış ve sıcaklık dağılımına etkisini hesaplamalı akışkanlar

dinamiđi (CFD) modelleriyle tespit etmiřtir, uygulamanın enerji tasarruf potansiyelini CFD sonularıyla desteklenen indirgenmiř termodinamik modellerle deđerlendirmek ve sistemin ekonomik potansiyeline y6nelik bir alıřma yapılmıřtır. Bu dođrultuda bir temsili veri merkezi d6ř6n6lmektedir;

- 1 MW kabin y6k6ne sahip temsili bir veri merkezinin EA ve OA, farklı tasarım parametreleri ve farklı BP y6ntemlerini kapsayan CFD modelleri oluřturulmuř. Bu modellerle CRAH BP y6nteminin oluřturduđu akıř ve sıcaklık dađlımlarından indirgenmiř modelleri destekleyecek veriler elde edilmiř.
- CRAH BP uygulamasıyla hava akıřı ve fan g6lerinin pratik tahmini iin akıř ađı modelleri (FNM) ve sođutma altyapısının enerji sarfiyatını tahmin etmek iin termodinamik modeller (TDM) oluřturulmuř. Hem FNM ve TDM modelleriyle hem de CFD sonuları g6z 6n6nde bulundurularak temsili veri merkezinin CRAH BP y6ntemiyle enerji optimizasyonu yapılmıř, farklı konfig6rasyonlarda indirgenmiř model yaklařımı (FNM ve TDM) ve CFD arasındaki optimizasyon sonuları karřılařtırılmıř.



1. INTRODUCTION

1.1 Background

A data center is a facility composed of server racks with the aim of processing and storing data. The data centers all over the world, specifically in U.S. comprise a remarkable part of energy consumption. Based on a recent investigation [1], in 2014, the calculated power use by data centers in U.S. was approximately 70 billion kWh or about 1.8% of total U.S. electricity consumption. This study shows from 2010 to 2014 the consumed electricity by data centers increased about 4%, the 24% rise calculated from 2005 to 2010. Power consumption in data centers is anticipated to keep this increasing trend from 2014 to 2020. Thus, the data centers require to devote a lot of effort to enhance energy efficiency.

The energy consumption by cooling systems in data centers may form half of the total energy usage and contributes significantly in total operating costs [2]. Therefore, decreasing cooling systems' power use can be considered an important parameter in improvement data centers energy efficiency. In a typical data center, usually a chilled water system as well as an airflow loop are used to respond the cooling demand (Figure 1.1 [3]). As a result, an optimized chilled water system accompanied with effective airflow management not only decrease the energy consumption and emission but also ensure reliable operation of IT equipment [2].

The server racks dissipate heat rapidly and need to keep the maximum temperature at server inlets below the 27°C, which is the recommended upper limit by the American Society of Heating Refrigerating and Air Conditioning Engineers (ASHRAE) [4]. Figure 1.2 provides the recommended range for data processing environments [4]. Otherwise overheating cause server racks to shut down or malfunction which is costly for business.

Generally air-cooled data centers consist in either hard-floor or raised-floor layout and server racks are typically located back to back and front to front in air-cooled data

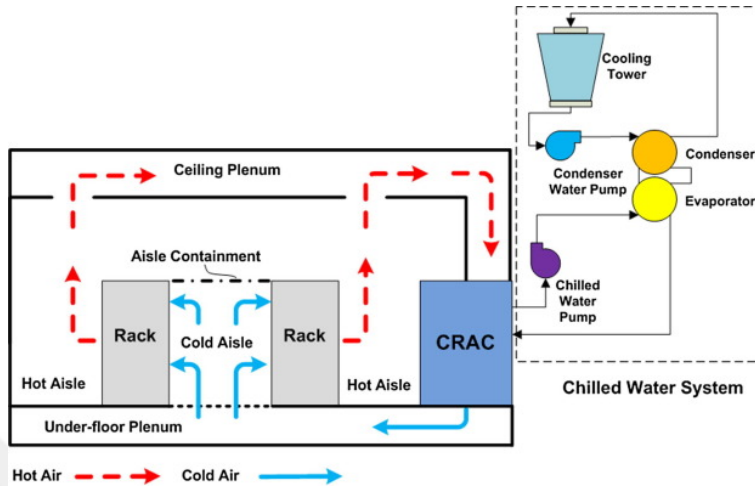


Figure 1.1 : Schematic of chilled water cycle and airflow loop in a raised-floor data center [3].

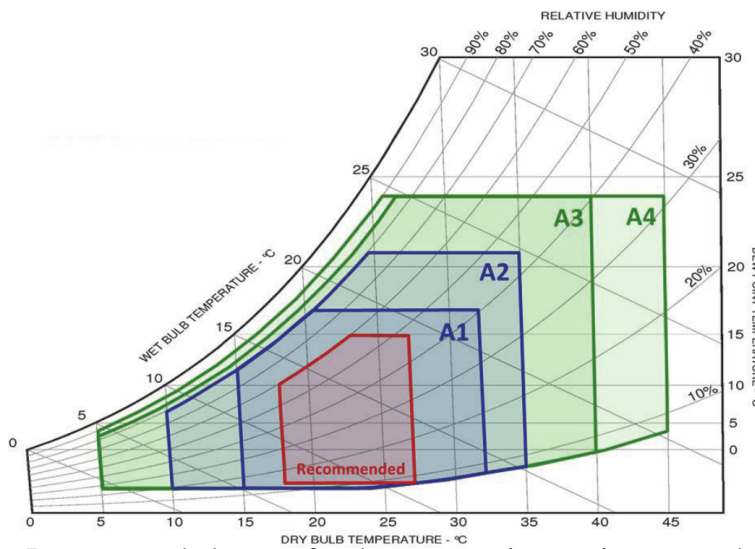


Figure 1.2 : Recommended range for data processing environments by ASHRAE.

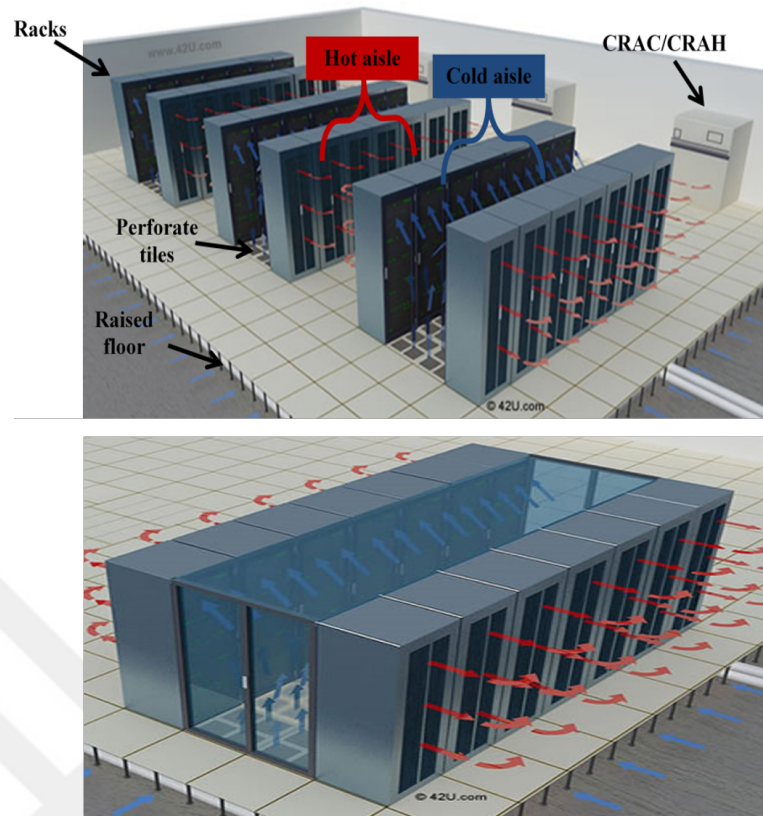


Figure 1.3 : Generic OA and EA data centers (www.42u.com)

centers to form hot and cold aisles. Figure 1.3 shows the schematics of a generic open cold aisle (OA) and enclosed aisle (EA) data center. In the raised-floor configuration the CRAH/CRAC (computer room air handling/conditioning) units in the data center supply cold airflow through the under-floor plenum to the cold aisles and draw return heated air from hot aisles. Since the flow field of air affects on the cooling of data center, monitoring temperature and flow fields in high power density and thermal loads is critical. Computational fluid dynamics (CFD) is a powerful tool to demonstrate elaborate information about temperature of various points as well as airflow pathlines with low costs.

In order to have uniform airflow across the server racks and higher cooling efficiency, in raised-floor data centers, preventing hot-air recirculation and cold-air BP is necessary. Effect of plenum height on the airflow velocity and pressure is frequently investigated by CFD method [2].

1.2 Literature Review

Power Usage Effectiveness (PUE) is the most widely used energy efficiency metric for data center infrastructure, which is the ratio of total facility energy consumption to that of the information technology (IT) equipment [5].

$$PUE = \frac{\text{Total facility energy consumption}}{\text{IT energy consumption}} \quad (1.1)$$

Despite considerable efforts regarding the data center energy efficiency, reports show more than 55% of studied cases had a PUE greater than 1.8 [6]. As a consequence of this survey, most data centers experience inefficient cooling systems and require effective air and thermal management.

Although several parameters can affect on temperature non-uniformity across the server racks, the air recirculation from hot aisle to cold aisle seems more important. Schmidt et al. [7] analyzed different parameters including ceiling and raised floor height, as well as the direction of airflow, which influence the cooling efficiency of air-cooled data centers. They concluded that mixing of cold and hot air is the main problem in raised-floor OA air-cooled data centers and leads to noticeable temperature non-uniformity at server inlets. CRAH units have to supply sufficient air flow for server racks, otherwise internal fans (inside the servers) draw airflow from above or around server racks into cold aisle which cause server racks to have higher temperatures at places with inadequate cold airflow.

Widely in OA data centers two methods including ceiling return vents and cold aisle containment might be applied to prevent air recirculation. In the ceiling return vent configuration, the airflow moves through designed paths above the hot aisles to the CRAH units. For a data center with the ceiling return vents Srinarayana et al. [8] showed the benefits of raised-floor in comparison with hard-floor data center. The another practical way to reduce the temperature non-uniformity is applying cold aisle containment. Enclosed cold aisle (EA) enables the cooling system to operate at a higher temperature possibly taking advantage of more free cooling hours. However, CRAH units in raised floor EA data centers have to supply the entire airflow for servers, as well as wasted airflow through the leakage paths and cable cutouts. Hence, an important part of cooling infrastructure energy consumption is due to the CRAH fans

[9]. In contrast, open cold aisle (OA) configuration may supply some part of required airflow by recirculating from hot aisles.

CRAH bypass (BP) method, recommended by Khalifa and Demetriou [10] [11] [12], decreases the CRAH air flow and provides the complementary fraction of the tile airflow either by forcing or inducing warm air from the hot aisle into the plenum using BP fans. This approach leads to significant reduction in the total fan power since the pressure BP fans need to overcome is typically an order of magnitude less than that CRAH fans do. However, reduced fan power does not guarantee optimum operation since the cooling system needs to operate at a lower temperature inefficiently to keep the rack inlet air temperatures below 27°C. Hence, there is a trade-off between the fan power and cooling power.

CFD tools enable us to model whole data center including raised-floor, perforated tiles, CRAH units and server racks. CFD simulation then ease the predicting temperature and flow fields for a data center. Also, it helps in implementing various ideas in order to obtain recommended cooling situation [13]. In order to trust CFD predictions, it should be validated with experimental measurements. Also, calibrating CFD model with experimental data is crucial before doing any parametric study [2].

Schmidt et al. [14] validated CFD method by an experiment at IBM Corporation in Poughkeepsie, NY. Patankar [13] investigated many physical parameters such as plenum height and porosity of perforated tiles with the help of CFD simulation. Bhopte et al. [15] through a numerical study demonstrated that increasing plenum height, in which static pressure variation in plenum decreases, causes more uniform air distribution in rack inlets. Moreover, they showed larger plenum depth reduces the hot-air recirculation space (declines the ceiling height) leading to higher cooling performance. A numerical study was conducted by Song [16] to investigate the effect of active tiles (perforated tiles associated with fan) in the data center. Abdelmaksoud et al. [17] experimentally and numerically studied perforated tiles. They tested experimentally performance of four perforated tiles, which their perforation changes from 25% to 56%, at a fixed flow rate and in an isothermal condition. According to the comparison of velocity profiles between perforated tiles and fully open tile, they suggested suitable CFD modeling for each tile. Despite numerous room-level CFD simulation studies, only a few included the use of fans underneath the perforated tiles.

Athavale developed an experimentally validated CFD model for a data center lab with active tiles and found that active tiles by changing plenum pressure influences on the CA airflow rate and amount of leakage from plenum into HA [18]. For a certain CRAC fan speed, a rise in active tile fan speed increases the passing airflow rate and declines the cold-air leakage in the plenum.

Nada and Said [19] experimentally and numerically studied how CRAC location and layout in a data center affect on airflow distribution. They resulted in that placing CRAC unit perpendicular to the rack row can cause higher cooling performance as well as more enhanced uniform airflow distribution. Emelie [20] used CFD modeling to assess the different cooling systems and find the best location of racks. Zhang et al. [21] in CFD simulation did not model inside of server racks and considered them like boxes. They resulted in that this kind of simplification does not lead to significant error with measurements. Almost in all studies coarse grid is employed for meshing data center. VanGilder et al [22] illustrated reducing mesh size from 6in to 1in caused little change and results were not independent of mesh size. Among various turbulence model the k- ϵ model is recommended for data center application [21]. Abdelmaksoud [17] proved that buoyancy effect should be considered in CFD modeling. In previous works, neglecting buoyancy effect can be the error source of CFD-estimated hot and cold spots.

Researchers studied CRAH BP method in various details through different modeling tools and experiments. Flow network modeling (FNM) is useful for predicting airflow rate and fan power especially for EA data centers [23] [24]. Erden et al. experimentally validated FNM in air-cooled data centers with and without BP with decent accuracy [25] [26]. FNM predictions of the airflow rate and fan power are within less than 10% of experimental measurements [26]. Even though Erden et al. [26] pointed out increasing temperature non-uniformity at higher BP fractions, they used well-mixed temperature assumption in the thermodynamic modeling (TDM) of the data center for optimization purposes in various previous studies [23] [24].

So far, relevant previous studies have been introduced. The next sections will explain the induced and forced CRAH bypass method in detail and talk about the main objective of this investigation.

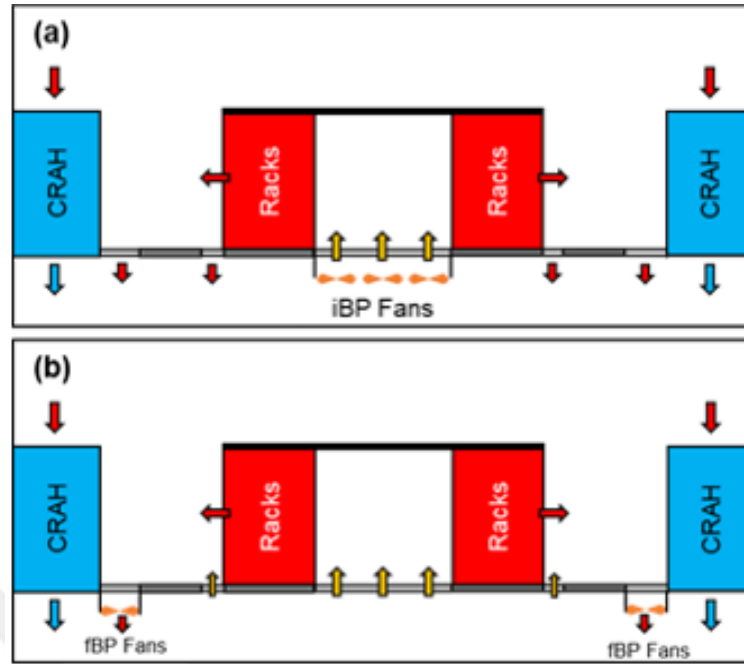


Figure 1.4 : Representative view of (a) induced and (b) forced BP configurations for air-cooled data centers.

1.3 Hypothesis

Figure 1.4 shows the schematics of two configurations of CRAH BP method, induced BP (iBP) and forced BP (fBP). In the iBP configuration, iBP fans are located just below the perforated tiles in the cold aisle (CA). At reduced CRAH flow rates, iBP fans compensate the reduced air flow by inducing room air through openings across the raised floor. These openings can be inherent leakage ports (e.g., cable cut-outs, tile seams, etc.) and intentional openings (e.g., perforated tiles in the hot aisle). The pressure in the plenum decreases at lower CRAH flow rates and even becomes lower than that of the room especially when CRAH flow rate is lower than rack air flow rate. Negative pressure in the plenum causes the room air to move from the room into the plenum eliminating the leakage airflow (Figure 1.4 a).

On the other hand, the fBP method consists of fBP fans underneath perforated tiles in the hot aisle (HA) preferably adjacent to the CRAH units. These fans maintain the positive plenum pressure when the CRAH fans run at lower speeds. Therefore, floor leakage remains intact. In contrast to the iBP fans that supply the entire rack airflow, fBP fans supply just a fraction of the rack airflow (Figure 1.4 b). Erden et al. [23] estimated five percentage points more reduction in cooling power by iBP compared to fBP using flow network modeling (FNM) for predicting fan power and thermodynamic

model (TDM) for estimating the chiller. Erden et al. [26] extended their work to build a unified modeling approach for iBP method and concluded as much as 52% reduction in the cooling power in data centers with indirect airside economizers utilizing iBP method.

1.4 Objectives

This study firstly tries to obtain a calibrated CFD model with respect to the available experimental results and then evaluates the CRAH BP method for various configurations including OA and EA in both of iBP and fBP data centers.

Erden [27] and Ahmadi and Erden [28] conducted the first CFD-based optimization studies for CRAH BP method and questioned the validity of the well-mixed temperature assumption in a quadrant of 1MW data center. Since their CFD results were not directly validated with any experimental data, obtaining reliable CFD model was necessary. This study includes the experimental validation of a CFD model against measured temperatures at Syracuse University's Green Data Center Research Laboratory (GDCRL) with iBP configuration. It is noteworthy, for this CFD model validation the different error sources for systematic and random errors are recognized and root mean square error (RMSE) values have been estimated. The following parametric study uses experimentally validated CFD model to evaluate the CRAH BP method impact on both iBP and fBP methods in the quadrant data center with and without aisle containment. In addition, CFD is used to test the well-mixed temperature assumption for a range of BP fractions and quantify the errors associated with this approach. A preliminary assessment by Erden shows that the temperature non-uniformities at larger BP fractions may lead to different results [27]. CFD modeling is an advantageous way to predict the complex airflow pattern and possibility of CRAH BP method for OA data centers. Moreover, CFD simulation is used to understand how variation of plenum height can affect on the energy consumption by cooling system, in which three different plenum heights have been considered. Eventually, this research investigates other parameters including three various IT loads and server airflow rates. As a result, this survey will present the energy saving potential of CRAH BP method with respect to the implemented configuration. In addition, the

current study will determine where the reduced-order model (TDM) is satisfactory and there is no need to do CFD study.





2. THEORY

2.1 Governing Equations

CFD method is a common approach for solving fluid mechanics equations that have a tough analytic solution. In the fluid flow and thermal environment, governing equations including conservation laws of mass, momentum and energy, and turbulence model equations may be stated in differential or integral form. Here, the differential form of the equations are discussed. Discretisation method turns differential equations into a system of algebraic equations. Among the most common discretisation methods (finite element, finite difference and finite volume) the Ansys Fluent uses finite volume method. This technique divides computational domain into small individually separate control volumes conserving macroscopic properties. For three dimensional geometries, the hexahedrons and tetrahedrons are considered as common shapes. Integrating governing equations over the control volume gives the discretized equations at computational cells. Then, by solving algebraic equations the flow properties can be calculated for all cells. Each properties of particles is a function of position and time.

The general form of all the governing equations is in the following form

$$\frac{\partial(\rho\phi)}{\partial t} + \frac{\partial(\rho u_i\phi)}{\partial x_i} = \frac{\partial(\Gamma_\phi \frac{\partial\phi}{\partial x_i})}{\partial x_i} + S_\phi \quad (2.1)$$

where ϕ is an arbitrary variable, ρ is the fluid density, u_i is the flow velocity (in x-component u, y-component v, z-component w), Γ_ϕ is the diffusion coefficient and S_ϕ is the source term. Also, in the above equation, the first term on the left hand side represents unsteady term and the second term shows convection term. The terms on the right hand side states the diffusion and source terms, respectively.

The conservation of mass or continuity equation for a compressible fluid flow is

$$\frac{\partial\rho}{\partial t} + \nabla \cdot (\rho u_i) = 0 \quad (2.2)$$

The first term states the rate of change of the density in time (mass per unit volume) and the next term represents the net rate of flow of mass out of the control volume through its boundaries. For an incompressible fluid flow the equation (2.2) becomes

$$\nabla \cdot u_i = 0 \quad (2.3)$$

According to the Newton's second law the rate of change of momentum of a fluid particle equals the sum of the forces on the particle. The forces on fluid particles consist of surface forces (pressure and viscous forces) and body forces (gravity, centrifugal, Coriolis and electromagnetic forces). The following equations demonstrate x,y and Z component of the momentum equations, respectively.

$$\frac{\partial(\rho u)}{\partial t} + \nabla \cdot (\rho u u_i) = \frac{\partial(-p + \tau_{xx})}{\partial x} + \frac{\partial \tau_{yx}}{\partial y} + \frac{\partial \tau_{zx}}{\partial z} + S_{Mx} \quad (2.4)$$

$$\frac{\partial(\rho v)}{\partial t} + \nabla \cdot (\rho v u_i) = \frac{\partial \tau_{xy}}{\partial x} + \frac{\partial(-p + \tau_{yy})}{\partial y} + \frac{\partial \tau_{zy}}{\partial z} + S_{My} \quad (2.5)$$

$$\frac{\partial(\rho w)}{\partial t} + \nabla \cdot (\rho w u_i) = \frac{\partial \tau_{xz}}{\partial x} + \frac{\partial \tau_{yz}}{\partial y} + \frac{\partial(-p + \tau_{zz})}{\partial z} + S_{Mz} \quad (2.6)$$

The first and second term on the left hand side shows the rate of change of momentum and the net flow of momentum out of the control volume, respectively. The terms on the right hand side state surface stresses (pressure and viscous stresses) and the rate of change of momentum due to sources.

The energy equation derived from the first law of thermodynamics represents that the rate of change of energy of a fluid particle is equal to the rate of heat addition to the fluid particle plus the rate of work on the particle. The following equation displays the energy equation

$$\begin{aligned} \frac{\partial(\rho E)}{\partial t} + \nabla \cdot (\rho E u_i) = & -\nabla \cdot (p u_i) + \left[\frac{\partial(u \tau_{xx})}{\partial x} + \frac{\partial(u \tau_{yx})}{\partial y} + \frac{\partial(u \tau_{zx})}{\partial z} + \frac{\partial(v \tau_{xy})}{\partial x} + \frac{\partial(v \tau_{yy})}{\partial y} \right. \\ & \left. + \frac{\partial(v \tau_{yz})}{\partial z} + \frac{\partial(w \tau_{xz})}{\partial x} + \frac{\partial(w \tau_{yz})}{\partial y} + \frac{\partial(w \tau_{zz})}{\partial z} \right] + \nabla \cdot (k \nabla T) + S_E \quad (2.7) \end{aligned}$$

The left hand side terms shows the rate of change of energy and the net flow of energy out of the volume, respectively. On the right hand side, the first term and the terms inside the bracket are due to the the total rate of work done by surface stresses. The last two terms display the rate of heat addition due to heat conduction through the boundaries of the control volume and the rate of change of energy due to sources.

Ansys Fluent provides condition to apply mass, momentum, energy and turbulent sources. Momentum sources as forces per unit volume acting on the fluid can only be specified on subdomains, not boundaries and points, and can be specified in different direction.

Also, Ansys Fluent using SIMPLE algorithm solves Reynolds-Averaged Navier-Stokes (RANS) equations for incompressible flow. The SIMPLE algorithm solves the velocity and temperature magnitudes via momentum and energy equations as scalar transport equations and resolves the pressure field by implicitly enforcing the continuity equation.

2.2 Turbulence Modeling

The Reynolds number, the ratio of inertial forces to viscous forces within a fluid, based on typical value for different situations determines the regime is laminar flow or turbulent flow. The turbulent flow regime is the dominant regime in industrial applications. This regime contains random fluctuations around the mean values of fluid properties and chaotic motion. Reynolds stresses in momentum equations stem from these fluctuations. In our particular problem, Ansys fluent uses RANS-based turbulence model to model the Reynolds stresses. Decomposing the flow variables into steady and a fluctuating component (Reynolds decomposition) gives the RANS equations

$$u(t) = \bar{u} + u'(t) \quad v(t) = \bar{v} + v'(t) \quad w(t) = \bar{w} + w'(t) \quad p(t) = \bar{p} + p'(t) \quad (2.8)$$

RANS equations including Reynolds stress terms are

$$\frac{\partial(\rho\bar{u})}{\partial t} + \nabla \cdot (\rho\bar{u}\bar{u}_i) = \frac{\partial(-\bar{p} + \tau_{xx} - \rho\overline{u'^2})}{\partial x} + \frac{\partial\tau_{xy} - \rho\overline{u'v'}}{\partial y} + \frac{\partial\tau_{xz} - \rho\overline{u'w'}}{\partial z} + S_{Mx} \quad (2.9)$$

$$\frac{\partial(\rho\bar{v})}{\partial t} + \nabla \cdot (\rho\bar{v}\bar{u}_i) = \frac{\partial\tau_{yx} - \rho\overline{u'v'}}{\partial x} + \frac{\partial(-\bar{p} + \tau_{yy} - \rho\overline{v'^2})}{\partial y} + \frac{\partial\tau_{yz} - \rho\overline{v'w'}}{\partial z} + S_{My} \quad (2.10)$$

$$\frac{\partial(\rho\bar{w})}{\partial t} + \nabla \cdot (\rho\bar{w}\bar{u}_i) = \frac{\partial\tau_{zx} - \rho\overline{u'w'}}{\partial x} + \frac{\partial\tau_{zy} - \rho\overline{v'w'}}{\partial y} + \frac{\partial(-\bar{p} + \tau_{zz} - \rho\overline{w'^2})}{\partial z} + S_{Mz} \quad (2.11)$$

The RANS-based turbulence models solves the problem based on the mean flow properties in the CFD. One of the most common and widely validated models, $k - \epsilon$

turbulence model, simulates mean flow characteristics and solves transport equations for the turbulence kinetic energy (k) and its dissipation rate (ε). The Boussinesq hypothesis used in the Spalart-Allmaras model, $k - \varepsilon$ model and $k - \omega$ relates Reynolds stress to the mean velocity gradients

$$-\rho \overline{u'_i u'_j} = \mu_t \left(\frac{\partial u_i}{\partial x_j} + \frac{\partial u_j}{\partial x_i} \right) \quad (2.12)$$

The mentioned transport equations are

$$\frac{\partial(\rho k)}{\partial t} + \frac{\partial(\rho k u_j)}{\partial x_j} = \frac{\partial \left[\left(\mu + \frac{\mu_t}{\sigma_k} \right) \frac{\partial k}{\partial x_j} \right]}{\partial x_j} - \rho \overline{u'_i u'_j} \frac{\partial u_j}{\partial x_i} + \beta g_i \frac{\mu_t}{Pr_t} \frac{\partial T}{\partial x_i} - \rho \varepsilon \quad (2.13)$$

$$\frac{\partial(\rho \varepsilon)}{\partial t} + \frac{\partial(\rho \varepsilon u_j)}{\partial x_j} = \frac{\partial \left[\left(\mu + \frac{\mu_t}{\sigma_\varepsilon} \right) \frac{\partial \varepsilon}{\partial x_j} \right]}{\partial x_j} + C_{1\varepsilon} \frac{\varepsilon}{k} \left(\mu_t \frac{\partial u_j}{\partial x_i} + C_{3\varepsilon} \beta g_i \frac{\mu_t}{Pr_t} \frac{\partial T}{\partial x_i} \right) - C_{2\varepsilon} \rho \frac{\varepsilon^2}{k} \quad (2.14)$$

where β is the thermal expansion coefficient ($\beta = 1/T$ for perfect gas), g_i is the gravitational body force, Pr_t is the turbulent Prandtl number for energy (the default value is 0.85), $C_{1\varepsilon}$, $C_{2\varepsilon}$ and $C_{3\varepsilon}$ are constants. σ_k and σ_ε represent turbulent Prandtl numbers for k and ε , respectively. The μ_t , turbulent viscosity, is computed from

$$\mu_t = \rho C_\mu \frac{k^2}{\varepsilon} \quad (2.15)$$

where C_μ is a dimensionless constant.

The experimental analysis have calculated the above mentioned constants

$$C_\mu = 0.09 \quad C_{1\varepsilon} = 1.44 \quad C_{2\varepsilon} = 1.92 \quad C_{3\varepsilon} = 1 \quad \sigma_k = 1 \quad \sigma_\varepsilon = 1.3$$

[29] [17] [20]

2.3 Near Wall Treatment

By increasing the distance from the solid wall, the fluid velocity increases. The Reynolds number based on the distance from the solid wall is defined as below,

$$Re = \frac{\rho U y}{\mu} \quad (2.16)$$

In other word, the Reynolds number is the ratio of inertial forces to the viscous forces. For regions far away from walls, the viscous forces are negligible and inertial forces due to momentum of the fluid are dominant. For areas noticeably close to the solid

walls, the range of Reynolds number is of order one. Here, the effect of viscous forces are more than or equal with inertial forces. This domain, which there is a linear relationship between the dimensionless velocity and wall distance, is called as linear or viscous sub-layer. The wall Y^+ estimated in CFD represents how the used near-wall mesh is fine or coarse;

$$u^+ = \frac{u\tau_y}{\nu} = y^+ \quad (2.17)$$

where y is the distance between wall and adjacent cell center, ν is the fluid kinematic velocity, and u_τ is the friction velocity or shear velocity defined as:

$$u_\tau = \sqrt{\frac{\tau_w}{\rho}} \quad (2.18)$$

In above equation the τ_w is the wall shear stress and ρ indicates fluid density. In drastically thin viscous sub-layer Y^+ is lower than 5. Since the logarithmic relationship between the dimensionless velocity and wall distance dominates in $30 < Y^+ < 500$ region, it is called log-law layer [29]. Wall functions or near-wall modeling are two approaches for areas adjacent to the wall. The first method employs semi-empirical formulas and is used in $k - \varepsilon$ model. Wall functions, to decrease the computational cost, instead of resolving the regions that viscous forces have effect ($Y^+ < 30$), link the solution between wall and fully turbulent flow. This method is appropriate for higher Reynolds number flows or coarse mesh close to the solid walls. However, the near-wall modeling approach is suitable for low Reynolds number flows with fine grid to resolve the viscous region [17]. This survey applies the wall function approach and considers $Y^+ < 500$ for CFD modeling.

2.4 Buoyancy

If added heat can affect on the fluid density, force of gravity cause fluid to be induced because of density variation. Such buoyancy-driven flows are called natural-convection (or mixed-convection) flows and can be modeled by ANSYS Fluent. To decide on the significance of buoyancy forces in a mixed convection flow (natural and forced convection) a dimensionless number called Archimedes number (Ar) is defined,

$$Ar = \frac{\beta g L \Delta T}{U^2} \quad (2.19)$$

where β is the thermal expansion coefficient ($\beta = 1/T$ for perfect gas), g is the gravitational acceleration, L is a characteristic vertical length scale (rack height), ΔT is the temperature difference between hot and cold aisles (airflow temperature rise by servers), and U is the characteristic velocity (average tile airflow velocity). When this number approaches or exceeds unity, buoyancy force influences on the flow. However, for Archimedes number around zero, the buoyancy force is negligible in comparison with inertia forces. In this study, β is equal with $1/T_{tile}$, rack height is considered as characteristic length, and U is obtained through the following equation:

$$U = \frac{Q_t}{A_t} \quad (2.20)$$

where Q_{tile} and A_{tile} are the flow rate and passing flow area for the perforated tiles, respectively. Moreover, for a data center operating at a certain IT load (P) and rack airflow (Q) the ΔT

$$\Delta T = \frac{P}{\rho c_p Q} \quad (2.21)$$

Different estimated Archimedes numbers through the various studied scenarios prove us that the buoyancy effect is important. CFD simulation employs the full buoyancy effect.

CFD modeling by ANSYS Fluent allows us to model the radiative heat transfer in data center. Walleed [17] proved that the amount of heat transfer by radiation from hot surfaces of server racks to the walls, ceiling and floor tiles is only 0.5% of racks generating heat. Thus, modeling such type of heat transfer easily can be avoided.

3. METHODOLOGY

3.1 CFD

To determine the temperature and flow field in the air space of data center, CFD models solve the mass (continuity), momentum and energy equations. The numerical simulation has been executed by using the commercially available, CFD software, Fluent 18.1, by applying the standard $k - \varepsilon$ turbulence model, standard wall function, and full buoyancy effects. The layouts of the 22 x 38 ft (6.71 x 11.58 m) quadrant of a generic data center (QDC) for both iBP and fBP configurations are in Figure 3.1 (top view). Moreover, the ceiling height above the raised floor and under-floor plenum height are 144 inches (3.66 m) and 36 inches (0.91 m), respectively. The dimensions of each floor tile are 24 x 24 inches (0.61 x 0.61 m).

QDC is made up of three halves and one whole CRAH units, stating 10 CRAH units for the whole data center. To represent CRAH units' exit condition at uniform temperature constant velocity inlet boundary condition is employed in the plenum. QDC with uniform IT load distribution has 20 racks in two rows housing 60 blade-type servers. In addition to usual boundary conditions such as velocity inlet, pressure outlet and wall, there is recirculation boundary condition which is specific to ANSYS FLUENT solver and is not available by default. Following commands are needed to active recirculation inlet and outlet boundary conditions:

```
(rpsetvar 'icepak?#t)
```

```
(models-changed)
```

This type of boundary condition is beneficial for modeling heating or cooling devices, in which one section supplies the fluid to the simulated device and the extracted fluid returns to the supply section. Depending on the type of application (cooling or heating), the recirculated fluid could be cooled down, heated up or returned at initial temperature [?].

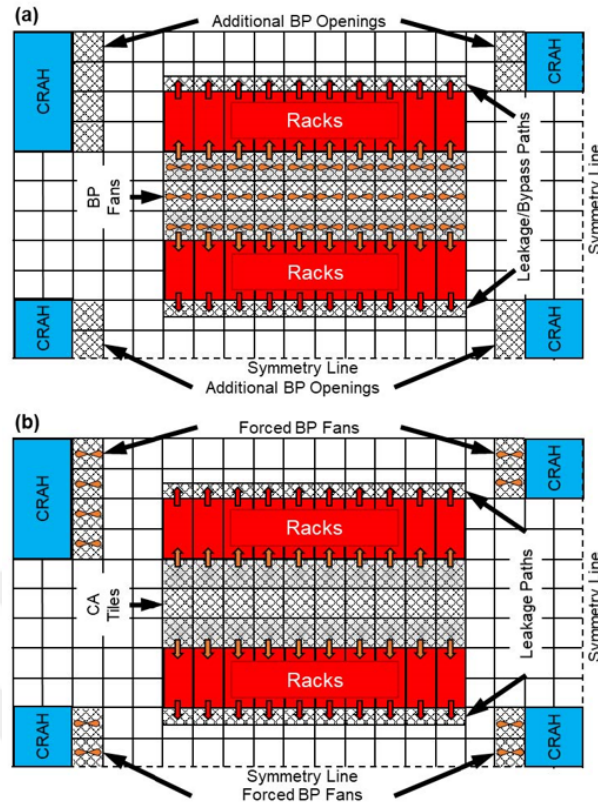


Figure 3.1 : Top view of the QDC layout for both (a) iBP and (b) fBP configurations.

The recirculation model allows reduced-order modeling of the server without the rack interior modeling and meshing. This model couples inlet and exit surfaces of each server, and to determine the exit boundary condition adds generated IT load heat to the inlet airflow. Figure 3.2 shows how the cold airflow has been heated up through the passing server racks. In this study, the rack inlets and outlets possess recirculation outlet and inlet boundary condition, respectively. The turbulence length for inlet boundaries is considered 7% of the hydraulic diameter of the opening [30], with typical values for turbulence intensity of 10% for servers [17] and 50% for CRAH units [12]. The CA in the QDC is 3-tile wide and 10-tile long. Two different openings enable airflow between the room and plenum in the rest of the floor. BP tiles are adjacent to CRAH units, and leakage tiles are at the back of the racks acting as cable cutouts. According to Erden et al. [26] all openings either in the cold aisle or hot aisle have a flow resistance coefficient of $K = 21$. A 4-inch (0.1016 m) thick porous volume assumes these openings with a porosity of 25% and the inertial resistance coefficient along the vertical flow direction. Based on whether iBP or fBP approach is in use, the location of CRAH BP fans changes in QDC. The BP fans in the iBP are in the cold

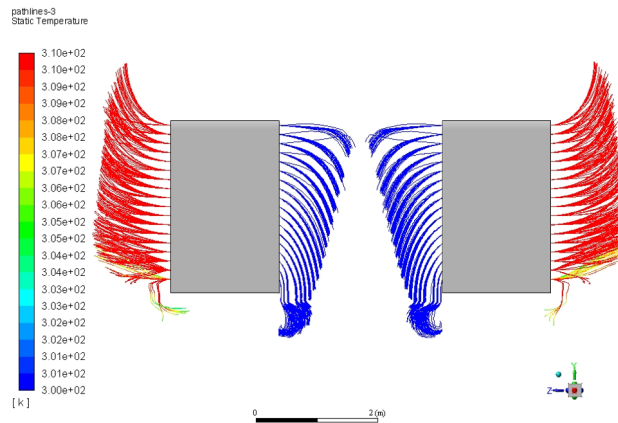


Figure 3.2 : Heating up cold airflow through the server racks.

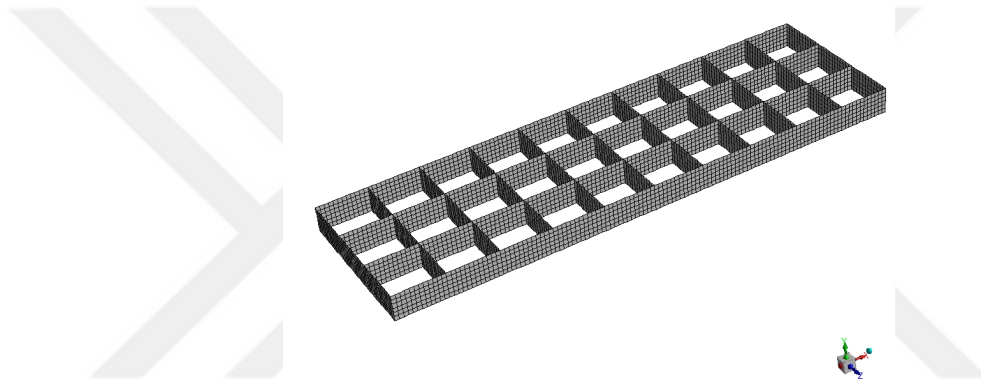


Figure 3.3 : Separating walls above the BP fan surfaces.

aisle underneath the perforated tiles (Figure 3.1 a) and in the fBP they are in the hot aisle only below the perforated tiles near to CRAH units (Figure 3.1 b).

As shown in Figure 3.3 the CFD model includes separating walls above the BP fan surfaces. The fan boundary condition, for both configurations, provides a constant pressure increase across the fan boundary surface, which is parallel to perforated tiles and placed 12 inches (0.3 m) away from the tiles inside the plenum. Moreover, this survey to create a complex flow pattern downstream and advanced mixing in BP fans use swirl-velocity specification (Figure 3.4). Ansys Fluent users should provide the direction vector of fans' rotation axis, as well as origin of fans in the global coordinate system. Also, fan hub radius, which is considered 0.08m, is necessary to active this fan feature. Generally, radial velocity is assumed zero, and the reasonable ratio of tangential velocity (V_t) to axial velocity (V_a) is around 1.0 ($V_t/V_a \sim 1$) [31]; however, to see the maximum effect of swirl specification, here ($V_t/V_a \sim 2$) is applied. Since for baseline QDC the airflow axial velocity is 1.27 m/s, the constant tangential velocity



Figure 3.4 : Airflow pattern with applying swirl-velocity specification.

equal with 2.54 m/s is used in CFD simulation. It is noteworthy, in spite of employing this amount the maximum difference in cooling power is only 3%.

According to the CFD study by Demetriou and Khalifa, the BP tiles neighboring to CRAH units provide more time for mixing and having more uniform temperatures at the cold aisle and rack inlets [12]. As a result, BP fans in fBP configuration as demonstrated in Figure 3.1 b are deliberately beneath perforated tiles next to CRAH units. Similarly, iBP has these intentionally-placed perforated tiles adjacent to CRAH units to induce room air into the plenum in addition to the inherent cable cutouts. Moreover, this research investigates all of the cases both with and without cold aisle containment (EA and OA).

3.1.1 Grid independency

In order to check the independency of numerical solutions of the mesh size, grid independency test should be performed. Grid independency happens when by refining the cell sizes, the numerical results no longer change considerably. The grid-independence study investigates five different grid sizes with the total number of cells ranging from about 100 thousand to 20 million to determine the sensitivity of mesh size to the results. The computational region for the QDC consists of hexahedral mesh with element sizes of 1&1, 2&2, 4&4, 4&2, 6&6 inches, in which the first and second numbers indicate the grid sizes at the room and plenum, respectively. The cases with uniform 4- and 6-inch mesh size require grid adaptation at the plenum walls to maintain y^+ values within recommended limits (i.e., $y^+ \leq 500$) [29]. Figure 3.5 compares the temperature at a particular point at the entrance of the CRAH unit for different number of cells. The 4&2 case provides reasonable computation time,

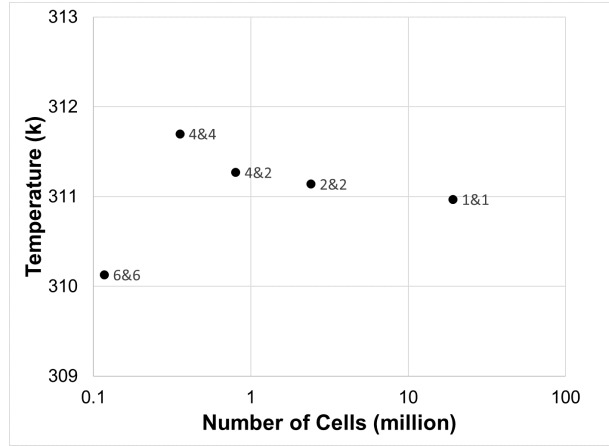


Figure 3.5 : Temperature variation of a particular point at the entrance of the CRAH unit in different number of cells.

and performance as the temperature difference between the finest mesh (1&1) is only 0.3°C. Moreover, the demonstrated temperature contours of rack inlets in Figure 3.6 for mentioned grid numbers proves that the selected 4&2 case has the the lowest difference with finest case.

3.2 TDM

Figure 3.7 shows simplified schematics of the FNM and TDM. The commercially available modeling tools, AFT Fathom [32] and TRNSYS [33], carry out the FNM and TDM, respectively. For baseline configuration, the flow network of data center excludes both iBP and fBP fans and the air flow path with the green line. CRAH BP configurations, iBP and fBP, have the air flow path with solid green line activated to allow the CRAH BP air flow in addition to the corresponding BP fans (i.e. iBP and fBP). In the FNM, the dominant flow resistances consist of the flow resistance of the CRAH units, racks, perforated tiles and leakage paths. The following equation estimates the pressure loss due to different resistances

$$\Delta P = \frac{1}{2} K \rho V^2 \quad (3.1)$$

where the K is the specific loss coefficient, ρ is the air density and V the air velocity. In order to calculate fan power, FNM employs the obtained pressure and flow distribution as well as relevant fan characteristics. Also, this survey assumes zero-static pressure for the room in data center. TDM resolves well-mixed air temperatures at key points (e.g., plenum, tile, rack exit, CRAH inlet/exit, etc.) by applying obtained fan flow rate and power use through FNM as well as setting redline temperature (27°C) at

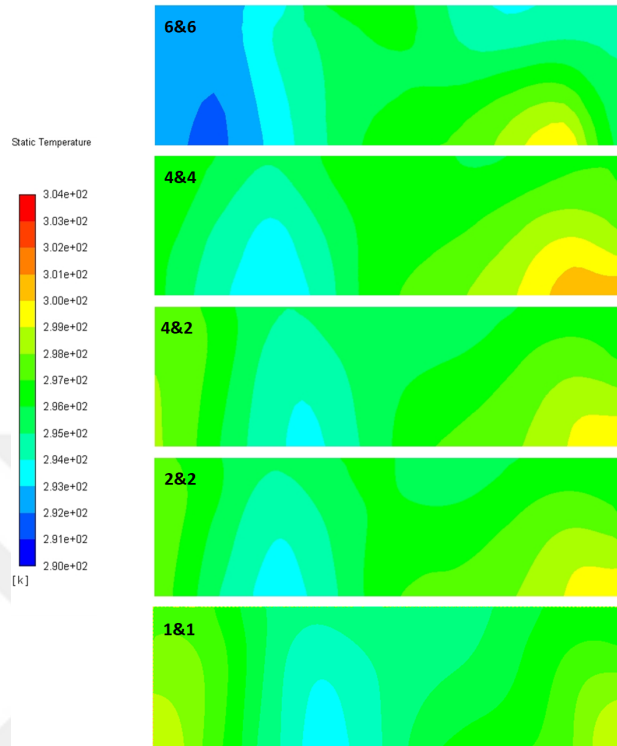


Figure 3.6 : Temperature contours of rack inlets in different number of cells.

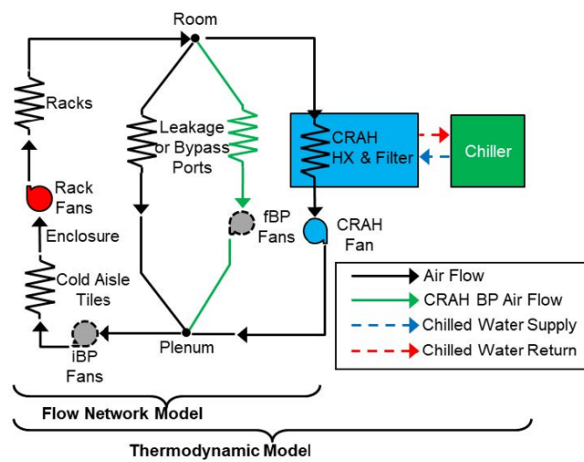


Figure 3.7 : Schematics of TDM and FNM.

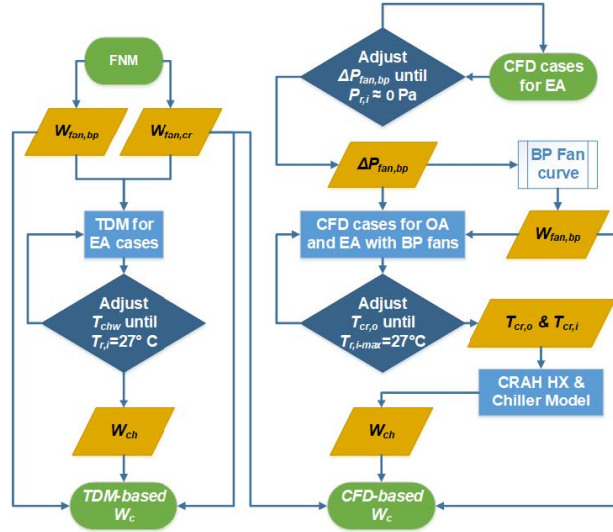


Figure 3.8 : Outline of TDM-based and CFD-based optimization.

server inlets. The ε -NTU relations gives the thermal effectiveness, ε , of the CRAH heat exchangers (HX) [34], where NTU is the ratio of the thermal conductance UA to the minimum of the fluid heat capacity ratios. At reduced CRAH air flow rates, UA scales with the 0.8th power of the flow rate according to the change of Nusselt Number for turbulent internal flow with Reynolds Number. Thus, HX model determines the chilled water temperature (T_{chw}) to be supplied by the chiller model. The chiller model computes the Coefficient of Performance (COP) and chiller power based on a normalized performance map at various chilled water setpoint temperatures [35] [36].

3.3 Optimization

For different CRAH-to-rack airflow ratios (ϕ) in both iBP and fBP with EA and OA data center, CFD analyses yield temperature and flow fields for QDC. Figure 3.8 demonstrates the outline of the TDM-based and CFD-based optimization of CRAH BP method for only EA data center [27] and for both EA and OA data centers, respectively.

It is necessary to provide zero-static pressure in rack inlets or inside the aisle containment. The CFD simulations for different values determine the required uniform static pressure increase through the BP fans (ΔP_{bp}). Knowing the pressure and airflow for BP fans, and applying the operating points and efficiency curves can lead to estimate BP fans power consumption ($W_{fan,bp}$). The obtained $W_{fan,bp}$ can cause a slightly temperature increase over the tiles equipped with BP fans. Hence, in CFD modeling it is an energy source input. Then, considering the maximum server rack

inlet temperature ($T_{r,i-max}$) under the redline (27°C), CFD gives the CRAH air supply temperature ($T_{cr,o}$). Finally, using the CRAH and chiller components of TDM shown in Figure 3.7, as well as the mass-weighted inlet and exit air temperatures at the CRAH unit, the chiller power, W_{ch} , can be determined. The ultimate cooling power is

$$W_c = W_{ch} + W_{fan,cr} + W_{fan,bp} \quad (3.2)$$

where CRAH fan power ($W_{fan,cr}$) is obtained by the FNM and BP fan power ($W_{fan,bp}$) is already based on CFD.

3.4 Model Assumptions

Table 3.1 specifies the features of 1 MW IT load data center. The similarly-divided IT load among the server racks increases temperature of rack airflow by 14.6°C ($\Delta T = 14.6^{\circ}\text{C}$). The cold aisle in entire data center includes 120 perforated tiles housing 120 BP fans in iBP configuration (Figure 3.1 a). As a main feature, CRAH BP configurations contain 40 perforated tiles in the HA near to CRAH units and in fBP configuration, 40 BP fans operate underneath these tiles (Figure 3.1 b). Furthermore, the leakage paths behind the racks with 40 perforated tiles cause roughly 25% of the CRAH air flow rate leakage into the room in the baseline configuration (i.e., $\phi = 1.33$). Key flow characteristics such as the resistances (CRAH, racks and tiles) and fan curves (CRAH, server and BP) are based on vendor data and in line with the assumptions in the previous optimization studies [24]. The thermal conductance UA for the cross-flow HX of a CRAH unit extracted from vendor catalog data is used by TDM model. Chiller cooling capacity is 1500 kW, has a COP of 6.0 and the condenser side receives cooling water at a temperature of 35°C .

Table 3.1 : Summary of Model Assumptions.

| Name | Value | Unit |
|---|-------|-------------|
| IT Power | 1000 | <i>KW</i> |
| Number of Racks | 80 | - |
| Rack Air Temperature Rise | 14.6 | °C |
| Number of CRAH Units | 10 | - |
| Single CRAH Rated Flow Rate | 8.02 | m^3/s |
| Single CRAH HX UA at the Rated Flow Rate | 16.0 | <i>KW/K</i> |
| CRAH Pressure Loss Factor, K_{cr} | 141 | - |
| Server Pressure Loss Factor, K_r | 205 | - |
| Perforated Tile Pressure Loss Factor, K_t | 21 | - |
| Number of Perforated Tile in the Cold Aisle | 120 | - |
| Number of iBP fans | 120 | - |
| Number of fBP fans | 40 | - |
| Chiller Rated Cooling Capacity | 1500 | <i>KW</i> |
| Design COP of the Chiller | 6.0 | - |
| Condenser Water Temperature | 35 | °C |

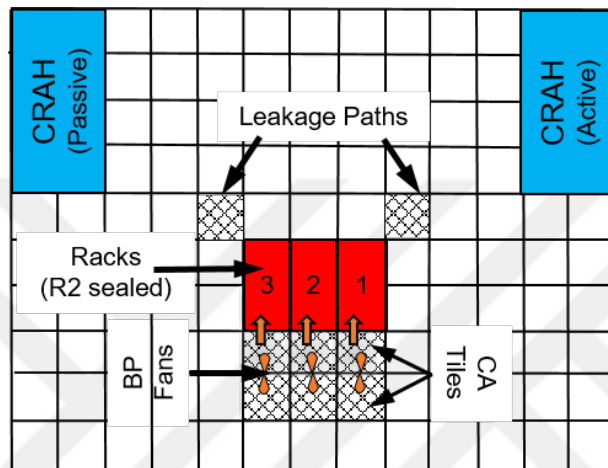


4. MODEL VALIDATION

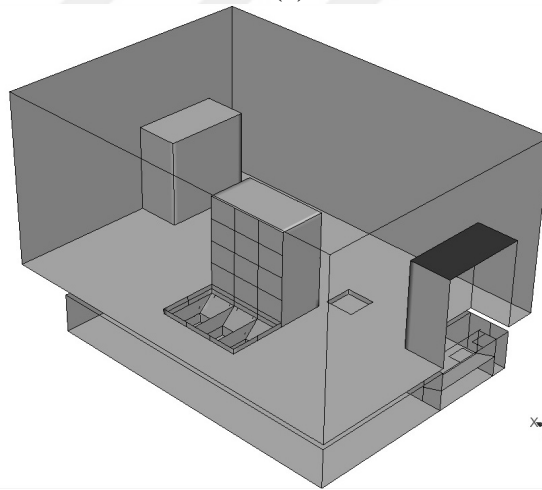
In order to validate the numerical model, the measured temperatures throughout the server rack inlets and leakages at the GDCRL have been compared with the CFD results. GDCRL consists of three simulated server racks, one of which was not operational. Two active racks generate a total power of 29.4 kW each with a total airflow rate of $1.151 \text{ m}^3/\text{s}$ (2440 CFM) leading to a temperature increase of $\sim 10.6^\circ\text{C}$. One of the two CRAH units with the flow capacity of $4.153 \text{ m}^3/\text{s}$ (8800 CFM) provides servers required airflow through the underfloor plenum. Single CRAH unit not only is sufficient for two active server racks but also decreases the experimental uncertainties. The plenum is approximately 1 m deep. CA consists of two rows of three perforated tiles. Two perforated tiles in the HA provide 25% of the CRAH airflow as leakage from the plenum into the room in the baseline case [26]. Figure 4.1 demonstrates the layout of experimental facility as well as its CFD model.

The shown picture in Figure 4.2 were taken from GDCRL [26]. Four thermocouple frames (each with nine thermocouples) remain at the top and bottom simulated chassis of R1 and R3 to monitor the server inlet air temperatures (Figure 4.2.a). The insulated portable cold aisle containment separates the HA and CA (Figure 4.2.b). Three commercially available fans installed below the six perforated tiles in CA, with around 0.5 m distance from plenum represents the BP fans of the iBP configuration (Figure 4.2.c).

An uncertainty (u) investigation quantifies the systematic (or bias) and random (or precision) error of the area-weighted average temperature over the server inlets and at the points exactly middle of the leakage tiles for the experimental data. According to the [17] the installed thermocouples on the wooden frames have a mean square error (MSE) around 0.11°C . The systematic or bias error consists of average MSE of the inlet temperatures (0.11°C), data acquisition error (DAQ) of ($\sim 0.025^\circ\text{C}$), CRAH exit temperature uncertainty error ($CRAH_{err}$) and the location bias error because of misaligned thermocouple frames (DT_{x-err} and DT_{y-err}) [37]. The expected sensor



(a)



(b)

Figure 4.1 : Experimental facility (a) layout, and (b) CFD model.



Figure 4.2 : Pictures of GDCRL (a) thermocouple frames, (b) portable cold aisle containment, and (c) installed fans below the perforated tiles in CA .

Table 4.1 : Calculation of bias error over the server inlets.

| | 0.54 | 0.63 | 0.67 | 0.81 | 0.99 | 1.33 |
|----------|-------|-------|-------|-------|-------|-------|
| MSE | 0.11 | 0.11 | 0.11 | 0.11 | 0.11 | 0.11 |
| DAQ | 0.025 | 0.025 | 0.025 | 0.025 | 0.025 | 0.025 |
| CRAH-err | 1.57 | 1.12 | 1.03 | 0.76 | 0.35 | 0.40 |
| DTx-err | 0.34 | 0.25 | 0.28 | 0.37 | 0.22 | 0.15 |
| DTy-err | 0.80 | 0.68 | 0.83 | 1.09 | 0.69 | 0.44 |
| Bias-err | 1.8 | 1.34 | 1.36 | 1.39 | 0.81 | 0.62 |

Table 4.2 : Total uncertainty error calculation over the server inlets.

| | 0.54 | 0.63 | 0.67 | 0.81 | 0.99 | 1.33 |
|-------------------|------|------|------|------|------|------|
| Random-err | 0.30 | 0.22 | 0.12 | 0.18 | 0.15 | 0.09 |
| Bias-err | 1.8 | 1.34 | 1.36 | 1.39 | 0.81 | 0.62 |
| Total uncertainty | 1.82 | 1.36 | 1.36 | 1.40 | 0.83 | 0.63 |

location errors are 1 and 2 inches in horizontal and vertical directions, respectively. Table 4.1 lists the final bias error magnitudes as well as its components for different ϕ values. In this table the combined bias error (u_b) is calculated as following equation:

$$u_b = \sqrt{(MSE)^2 + (DAQ)^2 + (CRAH_{err})^2 + (DT_{x-err})^2 + (DT_{y-err})^2} \quad (4.1)$$

Furthermore, the maximum STD (σ) values are estimated for the readings of the thermocouples at the server inlets. The maximum (u_p) precision error assumes 2σ ($\sim 95\%$ confidence interval) and forms the second term of total uncertainty [37]. Table 4.2 shows the random and bias errors as well as total uncertainty error for various ϕ values which is calculated by using following equation.

$$u = \sqrt{(u_b)^2 + (u_p)^2} \quad (4.2)$$

In addition to the sever inlets, this research repeats the same procedure for the measured temperatures at the center of both leakage tiles. Table 4.3 demonstrates the bias and random errors as well as total uncertainty errors for different ϕ values ranging from 0.54 to 0.99.

Generally, although all these mentioned factors contribute in the total uncertainty error, the uncertainty of CRAH exit air temperature ($CRAH_{err}$) drastically affect on it.

The operating CRAH unit in GDCRL has two small exit areas associated with the blowers and an angled vane to conduct the airflow towards the CA. Previous studies

Table 4.3 : Total uncertainty error calculation for leakage tiles.

| | 0.54 | 0.63 | 0.67 | 0.81 | 0.99 |
|-------------------|------|------|------|------|------|
| Random-err | 0.36 | 0.35 | 0.26 | 0.26 | 0.79 |
| Bias-err | 1.57 | 1.12 | 1.03 | 0.77 | 0.38 |
| Total uncertainty | 1.61 | 1.17 | 1.07 | 0.81 | 0.88 |

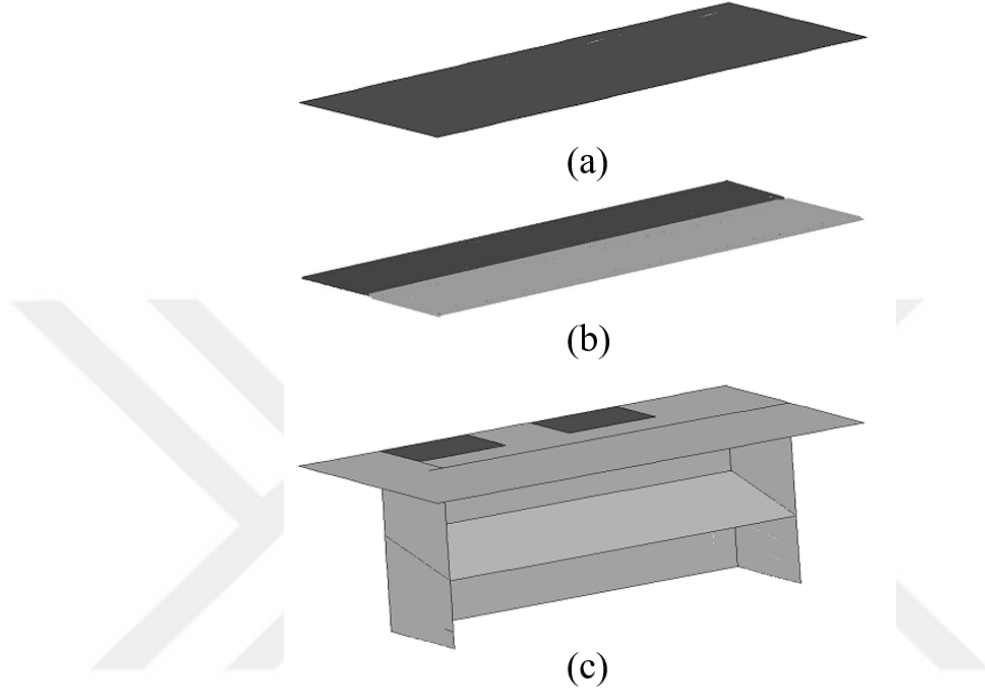
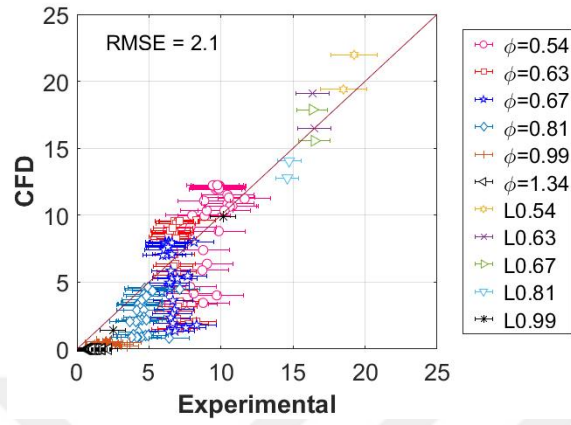


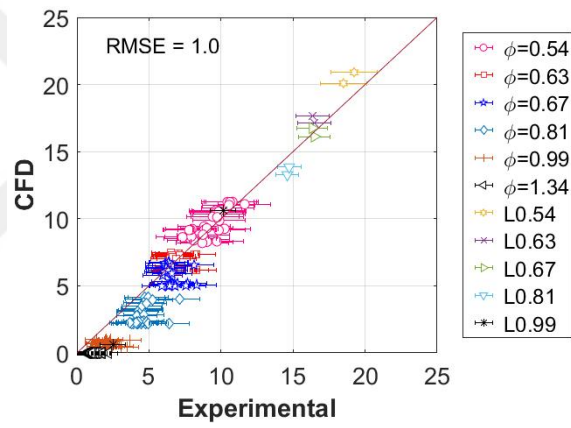
Figure 4.3 : Airflow exit area for three different cases (a) case 1, (b) case 2, and (c) case 3.

[27] [28] used the large opening at the entire floor area of the CRAH unit as the velocity boundary condition (Case 1). The model with the highest geometrical complexity includes the details of the CRAH exit and the vane structure (Case 3). In order to have a more representative momentum at the CRAH unit exit without the geometrical complexity of case 3, this work introduces another scenario with a narrow exit area (i.e., 16 in width) along the CRAH length (Case 2). It is noteworthy to mention that in case 2, CRAH airflow enters the domain with a 45-degree angle toward CA to have a similar directed flow due to the vane structure in case 3. However, the flow is downwards in Case 1. Figure 4.3 illustrates the area that airflow exits from CRAH unit in each of these three cases.

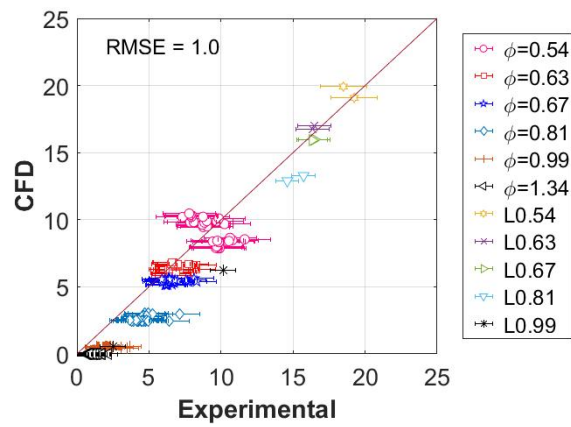
Figure 4.4 shows the comparison of experimental and CFD temperatures for cases 1, 2 and 3, respectively. In these figures, the written numbers in the legend parts correspond to the ϕ values and the word "L" indicates the leakage tile temperatures. The assumed



(a)



(b)



(c)

Figure 4.4 : Comparison of experimental and CFD temperatures for (a) case 1, (b) case 2, and (c) case 3.

error bars use the obtained uncertainty errors in this chapter. Also, root mean square error values are shown for each of cases. The numerically obtained temperatures correlate favorably with measured temperatures for case 3. For case 2 also there is a good agreement between CFD and experimental temperatures. However, for case 1 (fully open), the computational and experimental temperatures considerably deviate from each other which makes clear how the CRAH exit design in CFD noticeably influence on the rack inlet temperatures.





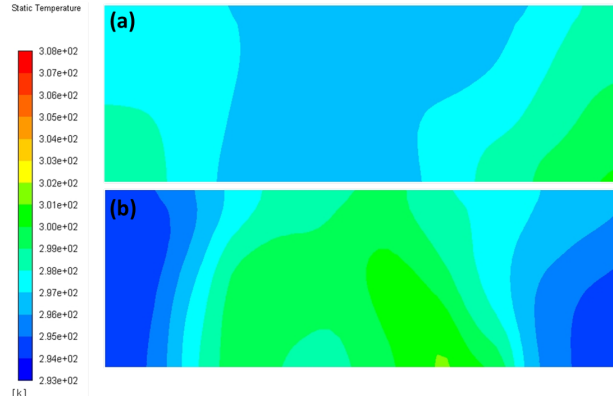


Figure 5.1 : Temperature contours of (a) case 2, and (b) case 1.

5. RESULTS AND DISCUSSION

The results section include CFD-based optimization results of the baseline data center given in Section 3.4 with an emphasis on the effect of CRAC exit boundary condition in parallel with the experimentally validated CFD. The subsequent parts not only examine how the optimum operating points and energy-saving potential of CRAH BP method in various configurations deviate from that of the baseline QDC configuration. Parametric studies of various designs and operating conditions include different plenum heights, IT load density and server airflow rate (temperature increase through the server racks). Also, the comparison of CFD and TDM results determines for which kind of studies CFD modeling is required.

5.1 CFD Versus TDM For The Optimization Of The Baseline QDC

In this part, this study firstly investigates the impact of CRAH exit designs including case 1 and case 2 (i.e., full area downward flow and narrow opening with a directed flow). Previous studies [27] [28] predicted higher temperature non-uniformities with the CRAH exit design case 1 at lower ϕ values compared to the results by experimentally validated CFD model with CRAC exit design case 2. Figure 5.1 illustrates the temperature contours for both of these cases at $\phi = 0.8$ in enclosed iBP configuration with same CRAH exit temperature, in which case 1 possesses higher temperature non-uniformities compared to the case 2.

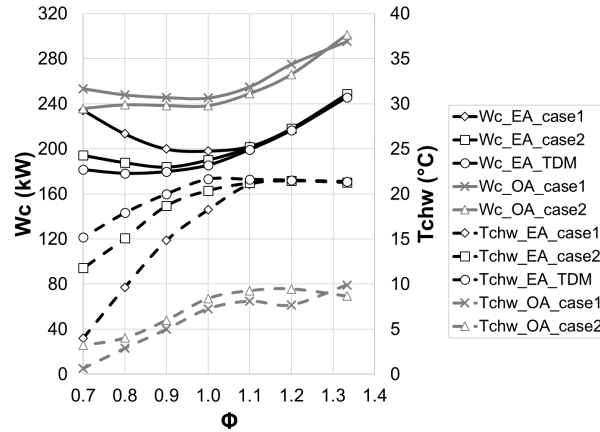


Figure 5.2 : Comparison of cooling power between CFD cases and TDM in iBP configuration.

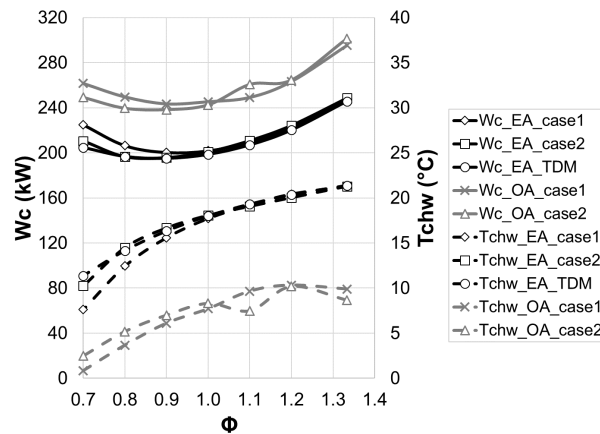


Figure 5.3 : Comparison of cooling power between CFD cases and TDM in fBP configuration.

Figure 5.2 and 5.3 present the cooling power (W_c) and the associated chilled water temperatures (T_{chw}) provided by TDM and CFD, for both iBP and fBP configurations, respectively. In these figures, the solid and dashed lines represent the W_c and T_{chw} , respectively. Figure 5.1 and 5.2 present the impact of CRAH exit flow area on the CFD-based optimization results for both CRAH exit design cases 1 and 2.

In iBP and fBP configurations of EA, the maximum differences for cooling power between the experimentally validated CFD and TDM, with well-mixed temperature and pressure assumptions, are 6.5% and 2.8%, respectively. At the optimal operating point, the difference is even lower than that. Due to the disagreement between the results and less time and effort in the TDM approach, TDM may be a robust technique to do some parametric studies in EA data centers.

On the other hand, CFD is the only option for the optimization of the CRAH BP for OA configuration, where the cooling system operates at lower evaporator temperatures

because of higher temperature non-uniformities. Even though the optimum value is $\phi = 0.9$ in fBP configuration, it is between $0.7 \leq \phi \leq 1$ for iBP configuration due to moderate fluctuations in this range.

5.2 Parametric Analysis

5.2.1 Plenum height

Variation of plenum height can lead to changes in velocity and pressure distribution inside the raised floor volume. By raising the plenum height, the pressure variations reduce and more uniform flow distribution appears as indicated in the literature [13]. This parametric study investigates three different plenum heights including 36 (baseline), 28, and 20 inches, and the impact of these scenarios on the CRAH BP method. Figure 5.4 compares the static pressure distribution of three mentioned cases at the plenum floor for $\phi = 0.8$ in EA data center with iBP configuration. This figure shows that the data center with lowest depth (20-inch) plenum has the most non-uniform pressure distribution. When the plenum height decreases the dynamic pressure in the plenum increases, particularly under the CA tiles where BP fans' wall placed. Therefore, rising the plenum height can eliminate pressure non-uniformities mainly generated by BP fans in the plenum.

Figure 5.5, 5.6 show the optimization results for EA and OA data centers with iBP and fBP configurations. In these figures, the solid black lines and dashed gray lines indicate the W_c on the primary axis and T_{chw} on the secondary axis, respectively.

For EA configurations shown in Figure 5.5 a and 5.6 a, the estimated cooling power for plenum heights of 36-inch is just under the 28-inch and the 20-inch scenario has the most cooling power due to the higher non-uniformity compared to others. Moreover, the EA CRAH BP case with 20-inch plenum has less potential to reduce cooling power compared to others. The estimated cooling power for iBP with OA configuration follows a similar trend observed for EA configuration (Figure 5.5 b). However, for fBP with OA configuration, the cooling power predictions do not follow a predictable pattern (Figure 5.6 b).

For both OA and EA configurations with iBP, the optimum ϕ values occur at the vicinity of 0.9. Regarding fBP configuration, the optimum values take place about

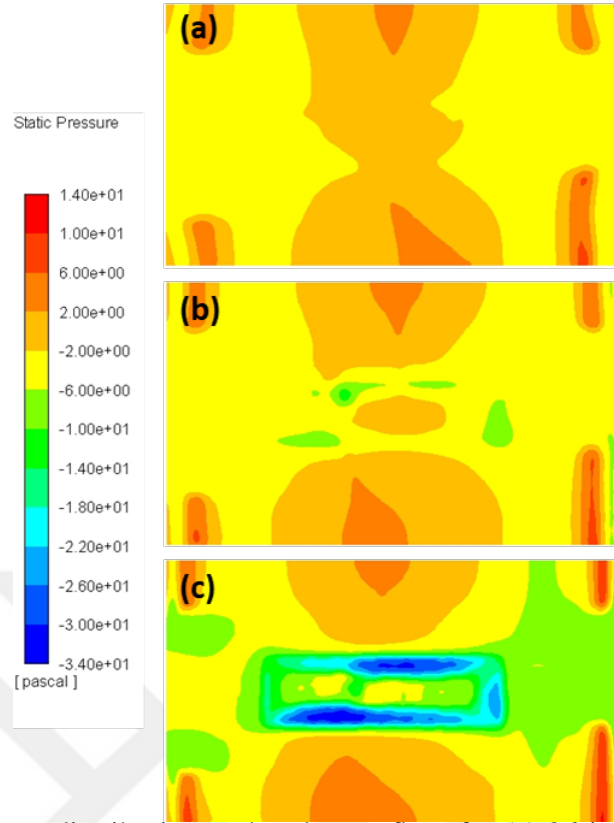
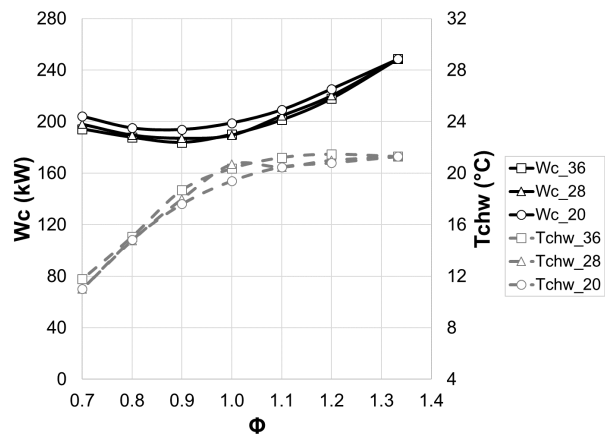


Figure 5.4 : Pressure distribution at the plenum floor for (a) 36-inch, (b) 28-inch, and (c) 20-inch plenum heights.

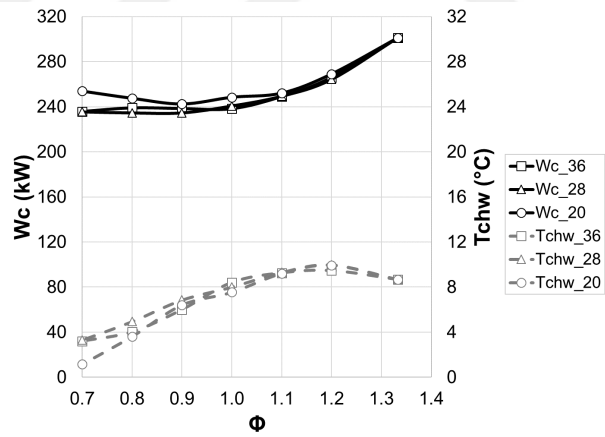
0.9 for 36 and 28-inch plenum heights in both EA and OA configurations. However, it is around $\phi = 1.0$ for the 20-inch case for OA with fBP. The error in the cooling power predictions by TDM compared to CFD is the highest in EA configuration with fBP (22%), where CFD use is further justified.

5.2.2 IT load and servers airflow temperature increase variations

Previous sections indicate reasonable agreement between the optimization results based on validated CFD and TDM in the baseline EA configuration. This section initially discusses the impact of variation in the server airflow rate on the temperature non-uniformities and optimization results. As the server airflow rate decreases the temperature difference across the racks (ΔT_{racks}) increases and there is a potential of increased temperature non-uniformity across the servers. Figure 5.7 demonstrates the biggest difference of 11% between the cooling power estimated by CFD and TDM, which is a confirmation of increased non-uniformity. Hence, CRAH BP applications in data centers with higher ΔT_{racks} and optimal ϕ values as low as 0.7 may require CFD analyses. On the other hand, there is less than 4.2% error in the cooling power

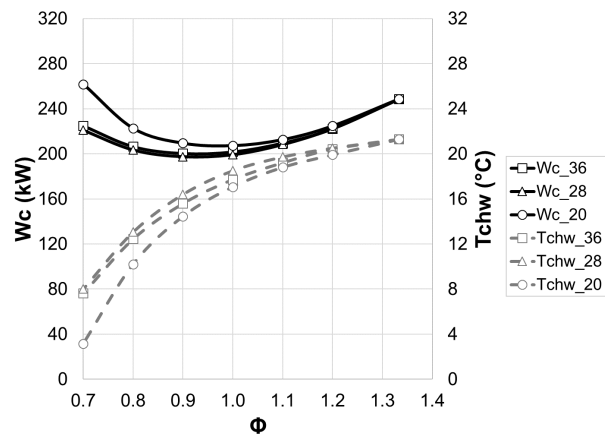


(a)

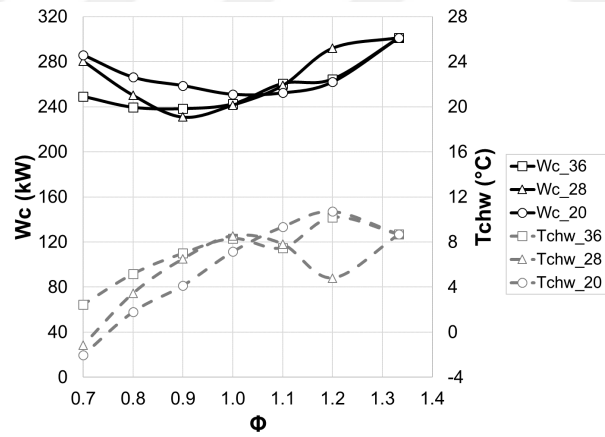


(b)

Figure 5.5 : Variation of plenum height for iBP configuration (a) EA and (b) OA data centers.



(a)



(b)

Figure 5.6 : Variation of plenum height for fBP configuration (a) EA and (b) OA data centers.

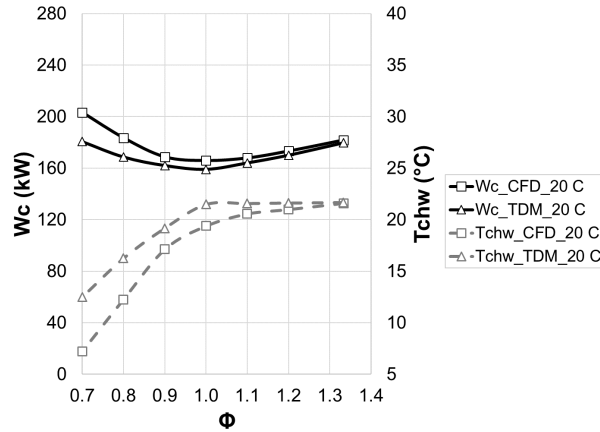


Figure 5.7 : Comparison of cooling power for $\Delta T = 20^{\circ}\text{C}$ by TDM and CFD in iBP configuration.

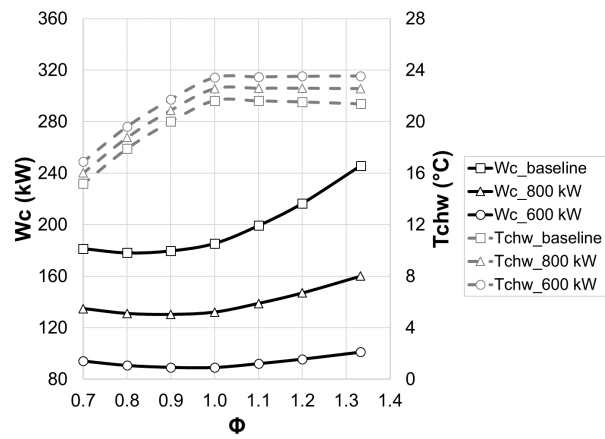
prediction by TDM at the optimal ϕ compared to the validated CFD. Considering the practicality of TDM, the ability to predict the optimal ϕ and the cooling power at the optimal ϕ with reasonable accuracy, TDM can still be considered as a decent tool for parametric analyses.

Figure 5.8 and 5.9 display the TDM-based optimization results of various levels of IT load and server airflow rate, respectively. In these figures, the solid and dashed lines indicate the cooling power (W_c) on the primary axis and the associated chilled water temperatures (T_{chw}) on the secondary axis, respectively. The baseline data center has 1000 kW IT load and $\Delta T_{racks} = 14.6^{\circ}\text{C}$.

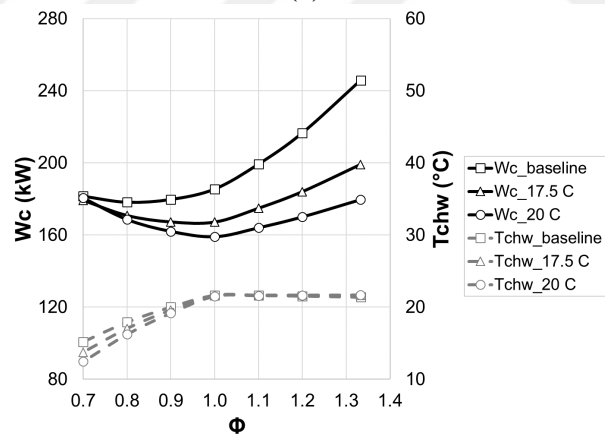
The scenarios of various IT load levels include 1000-kW (baseline), 800-kW and 600-kW in the same data center infrastructure for both iBP and fBP configurations. The energy saving potential is lower at lower load levels due to the oversized fan capacity and reduced fan power with reduced airflow requirement. The lowest influence is visible in 600-kW scenario where the cooling power reduces 11.7% and 5.5% for iBP and fBP, respectively. The optimum ϕ values in iBP configuration are 0.8, 0.9 and 1.0 for baseline, 800-kW and 600-kW cases, respectively. The optimum ϕ values are less sensitive to the load variations in fBP configuration, where $\phi = 0.9$ for the baseline and 800 kW cases and $\phi = 1.0$ for 600-kW case.

Discussion

This study responds to the some unaccomplished tasks in previous inquiries and determines where the CFD modeling can be avoided. Even though TDM is appropriate for some parametric studies such as variation of IT loads and servers airflow rates,

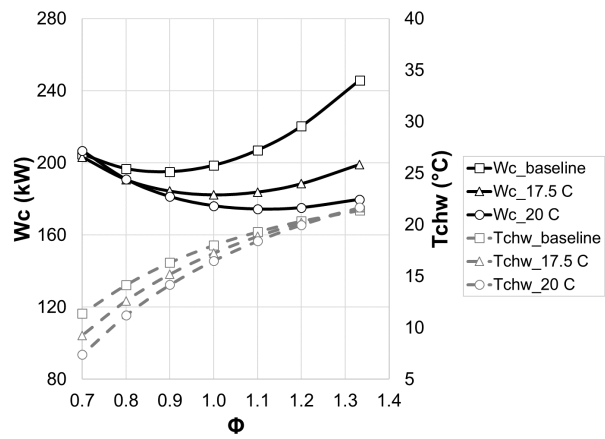


(a)

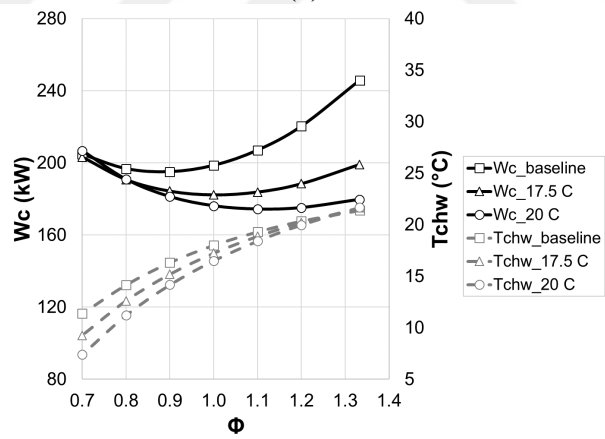


(b)

Figure 5.8 : Comparison of cooling power in iBP configuration for various (a) IT loads and (b) servers airflow rates.



(a)



(b)

Figure 5.9 : Comparison of cooling power in fBP configuration for various (a) IT loads and (b) servers airflow rates.

CFD modeling is necessary to examine the plenum height variation in data centers. The future work needs to establish the sensitivity of results to the various amount of leakage. Furthermore, impact of different number of fans as well as economic analysis of CRAH BP method should be addressed.

In order to evaluate the energy-saving potential of CRAH BP method, past studies assumed well-mixed pressure and temperature in FNM and TDM. According to the recent experimental investigations, despite acceptable performance of FNM in predicting the airflow rate and fan power, it does not adequately consider effects of temperature non-uniformities on the optimization results. The current research applies CFD method for different configurations in a range of CRAH BP fractions to estimate BP fan power and temperature non-uniformities. The obtained 14.7% and 1.5% relative standard deviation between FNM and CFD respectively for iBP and fBP represents FNM as a decent tool in predicting BP fan power. For $\phi \geq 1.0$ optimization results with TDM has a good agreement with CFD results in the EA data center. In contrast, for $\phi \leq 1.0$, CFD results significantly deviate from TDM, which assumes well-mixed temperature in modeling. The deviation is more considerable for iBP configuration rather than fBP. Based on CFD results, the optimum ϕ value is approximately 0.9 for all configurations. Around this value, the W_c related to the iBP decreases by 21% and 17% for EA and OA, respectively; likewise, 20% and 18% for fBP.

6. CONCLUSIONS

Data centers as one of the growing sectors over the world remarkably contribute in energy consumption. The power usage by cooling system in data centers forms approximately half of the entire energy consumption. CRAH fans account for a noticeable part of cooling system power use. CRAH BP method utilizes fan-equipped perforated tiles to induce or force room air through relatively lower flow resistance than that in CRAH units. Increasing the BP airflow rate reduces the total fan power and increases the chiller power since the CRAH unit needs to provide colder air when a certain fraction of warm room air is allowed to mix with cold CRAH airflow. Hence, there is a trade-off between the fan power and cooling power and finding the optimum operating point with respect to the various configurations is necessary.

The previous studies utilized reduced-order modeling tools (i.e. FNM and TDM) for the optimization of CRAH BP method, which assume uniform pressure and temperature at various zones in air-cooled EA data centers. Despite promising performance as a practical optimization tool, these tools ignore the impact of temperature and pressure non-uniformities on the optimization results and they cannot predict the performance of CRAH BP method in OA data centers with complex airflow patterns. Hence, CFD models are essential to investigate the CRAH BP method and evaluate the performance of TDM-based optimization tools. This study includes experimental validation of a CFD model to evaluate the energy-saving potential of CRAH BP method for iBP and fBP in both EA and OA configurations. In the CFD model validation, to have a more representative CRAH exit boundary condition without geometrical complexity, case 2 (i.e. narrow exit area with 16 inch width along the CRAH length) has been selected among three different cases.

Experimentally validated CFD results indicate instances (i.e., lower server air flow rates, shallow plenums) where reduced-order modeling tools exhibit higher errors in predicting optimal performance. This error is as high as 11% for $\phi = 0.7$ and less than 4.2% at the optimal ϕ for the baseline scenario. However, shallower plenums

and decreased airflow rate requirement by the servers further not only increase the temperature non-uniformities and but also decrease the potential for energy savings with CRAH BP method.



REFERENCES

- [1] **Shehabi, A., Smith, S., Sartor, D., Brown, R., Herrlin, M., Koomey, J., Masanet, E., Horner, N., Azevedo, I. and Lintner, W.** (2016). United states data center energy usage report.
- [2] **Chu, W.X. and Wang, C.C.** (2019). A review on airflow management in data centers, *Applied energy*, 240, 84–119.
- [3] **Song, Z.** (2017). Studying the fan-assisted cooling using the Taguchi approach in open and closed data centers, *International Journal of Heat and Mass Transfer*, 111, 593–601.
- [4] **ASHRAE**, (2015). Thermal Guidelines for Data Processing Environments, American Society of Heating, Refrigerating and Air-Conditioning Engineers, Atlanta, 4. edition.
- [5] **Belady, C., Rawson, A., Pfleuger, J. and Cader, T.** (2008). Green grid data center power efficiency metrics: PUE and DCIE, **Technical Report**, Technical report, Green Grid.
- [6] **Stansberry, M. and Kudritzki, J.** (2012). Uptime Institute 2012 data center industry survey, *Uptime Institute Survey*.
- [7] **Schmidt, R.R., Cruz, E. and Iyengar, M.** (2005). Challenges of data center thermal management, *IBM Journal of Research and Development*, 49(4.5), 709–723.
- [8] **Srinarayana, N., Fakhim, B., Behnia, M. and Armfield, S.** (2012). A comparative study of raised-floor and hard-floor configurations in an air-cooled data centre, *Thermal and Thermomechanical Phenomena in Electronic Systems (ITherm)*, 2012 13th IEEE Intersociety Conference on, IEEE, pp.43–50.
- [9] **Salim, M. and Tozer, R.** (2010). Data Centers' Energy Auditing and Benchmarking-Progress Update., *ASHRAE transactions*, 116(1).
- [10] **Khalifa, H. and Demetriou, D.** (2010). Energy optimization of air-cooled data centers, *Journal of Thermal Science and Engineering Applications*, 2(4), 041005.
- [11] **Khalifa, H.E. and Demetriou, D.W.**, (2012), Enclosed-aisle data center cooling system, uS Patent App. 13/191,509.
- [12] **Demetriou, D.W. and Khalifa, H.E.** (2012). Optimization of enclosed aisle data centers using bypass recirculation, *Journal of Electronic Packaging*, 134(2), 020904.

- [13] **Patankar, S.V.** (2010). Airflow and cooling in a data center, *Journal of Heat transfer*, 132(7), 073001.
- [14] **Schmidt, R.R., Karki, K.C., Kelkar, K.M., Radmehr, A. and Patankar, S.V.** (2001). Measurements and predictions of the flow distribution through perforated tiles in raised floor data centers, *Proceedings IPACK2001-15728*.
- [15] **Bhopte, S., Agonafer, D., Schmidt, R. and Sammakia, B.** (2006). Optimization of data center room layout to minimize rack inlet air temperature, *Journal of electronic packaging*, 128(4), 380–387.
- [16] **Song, Z.** (2015). Numerical Study for Data Center Cooling Using Active Tiles, *ASME 2015 International Mechanical Engineering Congress and Exposition*, American Society of Mechanical Engineers, pp.V08BT10A042–V08BT10A042.
- [17] **Abdelmaksoud, W.** (2012). Experimental and Numerical Investigations of the Thermal Environment in Air-Cooled Data Centers.
- [18] **Athavale, J., Joshi, Y. and Yoda, M.** (2018). Experimentally validated computational fluid dynamics model for data center with active tiles, *Journal of Electronic Packaging*, 140(1), 010902.
- [19] **Nada, S. and Said, M.** (2017). Effect of CRAC units layout on thermal management of data center, *Applied thermal engineering*, 118, 339–344.
- [20] **Wibron, E.** (2015). CFD Modeling of an Air-Cooled Data Center, *Master Degree, CHALMERS University of Technology, Gothenburg/Sweden*.
- [21] **Zhang, X., VanGilder, J.W., Iyengar, M. and Schmidt, R.R.** (2008). Effect of rack modeling detail on the numerical results of a data center test cell, *Thermal and Thermomechanical Phenomena in Electronic Systems, 2008. ITherm 2008. 11th Intersociety Conference on*, IEEE, pp.1183–1190.
- [22] **VanGilder, J.W. and Zhang, X.S.** (2008). Coarse-Grid CFD: The Effect of Grid Size on Data Center Modeling., *ASHRAE Transactions*, 114(2).
- [23] **Erden, H.S., Yildirim, M.T., Koz, M. and Khalifa, H.E.** (2016). Energy assessment of CRAH bypass for enclosed aisle data centers, *Thermal and Thermomechanical Phenomena in Electronic Systems (ITherm), 2016 15th IEEE Intersociety Conference on*, IEEE, pp.433–439.
- [24] **Erden, H.S., Koz, M., Yildirim, M.T. and Khalifa, H.E.** (2017). Optimization of Enclosed Aisle Data Centers With Induced CRAH Bypass, *IEEE Transactions on Components, Packaging and Manufacturing Technology*, 7(12), 1981–1989.
- [25] **Erden, H.S., Yildirim, M.T., Koz, M. and Khalifa, H.E.** (2016). Experimental investigation of CRAH bypass for enclosed aisle data centers, *Thermal and Thermomechanical Phenomena in Electronic Systems (ITherm), 2016 15th IEEE Intersociety Conference on*, IEEE, pp.1293–1299.

- [26] **Erden, H.S., Koz, M., Yildirim, M.T. and Khalifa, H.E.** (2017). Experimental demonstration and flow network model verification of induced CRAH bypass for cooling optimization of enclosed-aisle data centers, *IEEE Transactions on Components, Packaging and Manufacturing Technology*, 7(11), 1795–1803.
- [27] **Erden, H.S.** (2017). Investigation of induced CRAH bypass for air-cooled data centers using computational fluid dynamics, *Software, Telecommunications and Computer Networks (SoftCOM), 2017 25th International Conference on*, IEEE, pp.1–6.
- [28] **Ebrahimipour, V. and Erden, H.S.** (2018). Investigation of CRAH Bypass for Air-Cooled Data Centers using Computational Fluid Dynamics, *2018 IEEE International Telecommunications Energy Conference (INTELEC)*, IEEE, pp.1–6.
- [29] **Versteeg, H.K. and Malalasekera, W.** (2007). *An introduction to computational fluid dynamics: the finite volume method*, Pearson education.
- [30] **Chapter6**, (2018), ANSYS, Fluent 18.1 User Guide.
- [31] **Kromann, G., Pimont, V. and Addison, S.** (2010). CFD and EDA tools the interoperability of flotherm® and board station®/AutoTherm®: Concurrent design of a motorola powerPC™ RISC microprocessor-based microcomputer. Freescale Semiconductor, Inc.
- [32] **FATHOM9**. *Incompressible Pipe Flow Analysis and System Modeling Software, Appl. Flow Technol.*, Colorado Springs, CO, USA.
- [33] **Klein, S., Beckman, W., Mitchell, J., Duffie, J., Duffie, N., Freeman, T., Mitchell, J., Braun, J., Evans, B., Kummer, J. et al.** (2000). A transient system simulation program, *Solar Energy Laboratory, University of Wisconsin-Madison, Madison, WI, USA*.
- [34] **Bergman, T.L., Incropera, F.P., DeWitt, D.P. and Lavine, A.S.** (2011). *Fundamentals of heat and mass transfer*, John Wiley & Sons.
- [35] **Braun, J.** (1987). Performance and control characteristics of a large cooling system, *ASHRAE transactions*, 93(1), 1830–1852.
- [36] **Demetriou, D.W., Khalifa, H.E., Iyengar, M. and Schmidt, R.R.** (2011). Development and experimental validation of a thermo-hydraulic model for data centers, *HVAC&R Research*, 17(4), 540–555.
- [37] **Erden, H.S.** (2013). Experimental and analytical investigation of the transient thermal response of air cooled data centers, *Ph.D. thesis*.



CURRICULUM VITAE



Name Surname: Vahid Ebrahimpour Ahmadi

Place and Date of Birth: Tabriz, Iran, 5 December 1992

E-Mail: ahmadi17@itu.edu.tr

EDUCATION:

- **M.Sc.:** 2017-2019, Istanbul Technical University, Mechanical Engineering, Heat and Fluid
- **B.Sc.:** 2012-2016, Azerbaijan Shahid Madani University, Mechanical Engineering
- **B.Sc.:** 2013-2015, University of Tabriz, Mechanical Engineering (Exchange Student)

PUBLICATIONS, PRESENTATIONS AND PATENTS ON THE THESIS:

- Vahid Ebrahimpour Ahmadi, Hamza Salih Erden, 2018. Investigation of CRAH Bypass for Air-Cooled Data Centers using Computational Dynamics, *IEEE International Telecommunications Energy Conference, INTELEC 2018, Torino, Italy.*